Molecular Pharmacology Fast Forward. Published on December 12, 2022 as DOI: 10.1124/molpharm.122.000605
This article has not been copyedited and formatted. The final version may differ from this version.

MOLPHARM-AR-2022-000605

TITLE PAGE

Mutual Cooperativity of Three Allosteric Sites on the Dopamine D1 Receptor

Xushan Wang, Erik J Hembre, Paul J Goldsmith, James P Beck, Kjell A Svensson, Francis S Willard*, Robert F Bruns

Lilly Research Laboratories, Eli Lilly & Co., Lilly Corporate Center, Indianapolis, Indiana.

Downloaded from molpharm.aspetjournals.org at ASPET Journals on April 20, 2024

Molecular Pharmacology Fast Forward. Published on December 12, 2022 as DOI: 10.1124/molpharm.122.000605
This article has not been copyedited and formatted. The final version may differ from this version.

RUNNING TITLE PAGE

Three Allosteric Sites on the Dopamine D1 Receptor

Address correspondence to: Dr. Francis Willard, Lilly Research Laboratories, Eli Lilly & Co., Lilly Corporate Center, Indianapolis, IN 46285, USA. 317 276-8786. Email: willardfs@lilly.com

Number of text pages: 49

Number of tables: 4

Number of figures: 9

Number of references: 42

Number of words in Abstract: 194

Number of words in Introduction: 718

Number of words in Discussion: 2,044

Nonstandard abbreviations: CRC, concentration-response curve; ECL, extracellular loop; ICL, intracellular loop; NAM, negative allosteric modulator; PAM, positive allosteric modulator; TMH, transmembrane helix

Downloaded from molpharm.aspetjournals.org at ASPET Journals on April 20, 2024

Molecular Pharmacology Fast Forward. Published on December 12, 2022 as DOI: 10.1124/molpharm.122.000605
This article has not been copyedited and formatted. The final version may differ from this version.

ABSTRACT

An amine-containing molecule called Compound A has been reported by a group from Bristol-Myers Squibb to act as a positive allosteric modulator (PAM) at the dopamine D1 receptor. We synthesized the more-active enantiomer of Compound A (BMS-A1) and compared it with the D1 PAMs DETQ and MLS6585, which are known to bind to intracellular loop 2 and the extracellular portion of transmembrane helix 7, respectively. Results from D1/D5 chimeras indicated that PAM activity of BMS-A1 tracked with the presence of D1 sequence in the N-terminal/extracellular region of the D1 receptor, a unique location compared to either of the other PAMs. In pairwise combinations, BMS-A1 potentiated the small allo-agonist activity of each of the other PAMs, while the triple PAM combination (in the absence of dopamine) produced a cAMP response about 64% of the maximum produced by dopamine. Each of the pairwise PAM combinations produced a much larger leftward shift of the dopamine EC_{50} than either single PAM alone. All three PAMs in combination produced a 1,000-fold leftward shift of the dopamine curve. These results demonstrate the presence of three non-overlapping allosteric sites that cooperatively stabilize the same activated state of the human D1 receptor.

SIGNIFICANCE STATEMENT

Deficiencies in dopamine D1 receptor activation are seen in Parkinson's disease and other neuropsychiatric disorders. In this study, three positive allosteric modulators of the dopamine D1 receptor were found to bind to distinct and separate sites, interacting synergistically with each other and dopamine, with the triple combination causing a 1,000-fold leftward shift of the response to dopamine. These results showcase multiple opportunities to modulate D1 tone and highlight new pharmacological approaches for allosteric modulation of GPCRs.

Downloaded from molpharm.aspetjournals.org at ASPET Journals on April 20, 2024

Molecular Pharmacology Fast Forward. Published on December 12, 2022 as DOI: 10.1124/molpharm.122.000605
This article has not been copyedited and formatted. The final version may differ from this version.

INTRODUCTION

G-protein coupled receptors (GPCRs) transduce the biological signals of numerous hormones, growth factors, and neurotransmitters, thereby representing the largest single class of druggable human proteins (Santos et al., 2017; Alexander et al., 2021). Traditional pharmacological approaches for targeting GPCRs have involved identifying small molecule drugs that occupy the same pocket as the natural ligand (orthosteric agonists or antagonists). However, accumulating biochemical and structural data indicates that GPCRs may have additional (allosteric) ligand binding pockets that can modulate receptor function either positively (positive allosteric modulator, PAM) or negatively (negative allosteric modulator, NAM) (Stockton et al., 1983; Bruns and Fergus, 1990; May et al., 2007). PAMs affect receptor activation by modulating the binding affinity and/or efficacy of the orthosteric ligand and, at higher concentrations, can directly activate receptors. As therapeutics, PAMs have potential advantages over orthosteric agonists because their actions are largely dependent on the presence of endogenous agonist, which is under physiological control (May et al., 2007; Kenakin, 2010). Mechanistically, PAMs operate by binding selectively to the activated state of the receptor (Bruns and Fergus, 1990; Ehlert, 2016), driving the thermodynamic equilibrium toward activation, whereas NAMs have the reverse selectivity. In theory then, any site that changes its configuration between the active and inactive states could host an allosteric modulator, and several such sites have been identified on various GPCRs (Thal et al., 2018).

The D1 receptor is the most highly expressed of the five dopamine receptors (Beaulieu and Gainetdinov, 2011). Although deficiencies in D1 activation are associated with various CNS disorders such as Parkinson's disease and schizophrenia (Ikemoto et al., 1997; Nakamura et al., 2014; Arnsten et al., 2017), attempts to develop D1 agonists have been hampered by issues

Downloaded from molpharm.aspetjournals.org at ASPET Journals on April 20, 2024

Molecular Pharmacology Fast Forward. Published on December 12, 2022 as DOI: 10.1124/molpharm.122.000605
This article has not been copyedited and formatted. The final version may differ from this version.

including tolerance development, pharmacokinetic limitations, and limited selectivity (Felsing et al., 2019; Svensson et al., 2019). To overcome these problems, we (Svensson et al., 2017; Bruns et al., 2018) and others (Lewis et al., 2015; Shiraki et al., 2015; Luderman et al., 2018) have identified various chemical series with D1 PAM activity (Figure 1). Among these are two members of the tetrahydroisoquinoline (THIQ) class of D1 PAMs, the pharmacological tool DETQ and the phase II clinical molecule LY3154207 (USAN name mevidalen) (Hao et al., 2019; Biglan et al., 2022).

To date, two separate binding sites for D1 PAMs have been reported. The most well-characterized of these is the inner surface of intracellular loop 2 (ICL2) along with adjacent parts of transmembrane helices (TMH) 3 and 4. Mutations in this region have marked effects on the affinity of several D1 PAMs, including DETQ as well as compounds from two other structural series (Lewis et al., 2015; Luderman et al., 2018; Wang et al., 2018). LY3154207 has been imaged in the ICL2 site by cryo electron microscopy (Xiao et al., 2021; Zhuang et al., 2021; Teng et al., 2022).

In contrast, the D1 PAM activity of MLS6585 is unaffected by mutations to the ICL2 site (Luderman et al., 2018; Wang et al., 2018). MLS6585 was shown to interact supra-additively with DETQ and other ICL2-binders, confirming that it binds to a separate site. In agreement with this observation, the binding site for MLS6585 has recently been reported to include the extracellular portion of TMH7 (Luderman et al., 2021).

In 2015, a group from Bristol-Myers Squibb described two D1 PAMs, Compound A and Compound B. Compound B was shown to bind to ICL2, but the binding site for Compound A was not characterized, other than excluding the possibility that it bound to ICL2 (Lewis et al., 2015).

Downloaded from molpharm.aspetjournals.org at ASPET Journals on April 20, 2024

Molecular Pharmacology Fast Forward. Published on December 12, 2022 as DOI: 10.1124/molpharm.122.000605
This article has not been copyedited and formatted. The final version may differ from this version.

In the current study, we synthesize Compound A and separate the more active enantiomer, which we abbreviate as BMS-A1. Using D1/D5 chimeras, we show that BMS-A1 binds to the N-terminal/extracellular region of the D1 receptor, distinct from ICL2 binders (N-terminal/intracellular) and MLS6585 (C-terminal/extracellular). Pairwise and triple combinations between DETQ, MLS6585, and BMS-A1 in the absence of dopamine show greatly increased allosteric agonist activity, confirming that they occupy distinct binding sites on the D1 receptor that are functionally cooperative. Moreover, dual and triple combinations of the three PAMs synergistically enhance the functional affinity of the orthosteric agonist dopamine, causing a leftward shift of up to 1,000-fold in the dopamine EC_{50} in the triple combination. These results provide the first evidence that a functional four-ligand GPCR complex can be formed, with potential implications for GPCR pharmacology, allostery, and drug discovery.

Downloaded from molpharm.aspetjournals.org at ASPET Journals on April 20, 2024

Molecular Pharmacology Fast Forward. Published on December 12, 2022 as DOI: 10.1124/molpharm.122.000605
This article has not been copyedited and formatted. The final version may differ from this version.

MATERIALS AND METHODS

Materials. DETQ was synthesized as previously described (Beadle et al., 2014; Hao et al., 2019). MLS6585, called CID 2886111 in our previous paper (Wang et al., 2018), was purchased from ChemBridge (San Diego, CA, USA). The more-active enantiomer of Bristol-Myers Squibb Compound A was synthesized at Eli Lilly and Company (Supplemental Data II: Synthesis of BMS-A1 and Stereoisomers). Dopamine and other pharmacological reagents were purchased from Sigma (St. Louis, MO, USA). Sources of other reagents are provided in individual protocols.

HEK293 cell line expressing the human D1 receptor. All experiments except those involving D1/D5 chimeras were carried out in a stable HEK293 cell line expressing the human D1 receptor, as previously described (Svensson et al., 2017). This cell line shows a moderate level of D1 receptor expression (B_{max} 0.36 pmol/mg protein in ^{3}H-SCH 23390 binding) and allo-agonist activity of DETQ and MLS6585 is relatively low compared to the Jump-in expression system used for the D1/D5 chimeras (Wang et al., 2018).

D1/D5 chimera cell lines. Human D1/D5 chimeras were constructed as previously described (Wang et al., 2018). Human DRD1 and DRD5 cDNA constructs were purchased from Open Biosystems, Huntsville, AL, USA and ThermoFisher (Waltham, MA, USA), respectively. D1/D5 chimera DNA was synthesized by GenScript (Piscataway, NJ, USA). All constructs were verified by DNA sequencing. Switchover points for all chimeras are described in the Supplemental Data in (Wang et al., 2018). Stable cell lines were established using the Jump-In™ T-REx™ HEK293 Retargeting Kit (ThermoFisher). Wild-type and chimera constructs were either directly cloned into pJTI R4 CMV-TO vector or sub-cloned from pcDNA3.1, then transfected using Fugene HD into Jump-In™ T-REx™ HEK293 cells. Transfected cells were selected using 2.5 mg/ml G418 for 10 to 14 days. Stable cells were induced using 1 µg/ml doxycycline for 24 to 48 hours, then harvested and suspended in freeze media (FBS with 6%

Downloaded from molpharm.aspetjournals.org at ASPET Journals on April 20, 2024

Molecular Pharmacology Fast Forward. Published on December 12, 2022 as DOI: 10.1124/molpharm.122.000605
This article has not been copyedited and formatted. The final version may differ from this version.

DMSO) at 10^7 cells/ml, and aliquots were stored in liquid nitrogen. Receptor expression levels in the Jump-In system were typically around 5 pmol/mg protein, or roughly 10-fold higher than in the D1 cell line used for α-shift experiments (Wang et al., 2018).

Measurement of cAMP response. Cyclic AMP experiments were carried out as previously described (Svensson et al., 2017; Wang et al., 2018) with minor modifications. In the D1/D5 chimera studies, BMS-A1 was diluted and dispensed into assay plates in 80 nL DMSO (ProxiPlate-384 Plus, PerkinElmer, Waltham, MA, USA) using acoustic dispensing (Echo, Beckman Coulter, San Jose, CA, USA). Dopamine was dissolved and diluted in DMSO and dispensed in a 10 nL volume (final assay volume 10 µL). In preliminary experiments, a separate dopamine EC_{20} value was determined for each construct (Wang et al., 2018). An 8 µM final concentration of dopamine was used for the EC_{max}. The final DMSO concentration was 0.9%. Curve shift experiments were carried out in the stable HEK293 D1 cell line described above. The first PAM (DETQ or BMS-A1) was diluted and dispensed into assay plates (ProxiPlate-384 Plus, PerkinElmer, Waltham, MA, USA) using acoustic dispensing with a two-fold dilution factor in a 14-point curve in 80 nL DMSO to rows A through N. Dopamine was diluted and dispensed into the assay using acoustic dispensing with a two-fold dilution factor and 20-point curve in 80 nL DMSO to columns 3 through 22. The second or/and third potentiator compound was dispensed into assay plates using acoustic dispensing in 20 nL DMSO to reach final concentration in a 10 µl reaction volume. Diluted compound and dopamine were resuspended with 5uL STIM buffer, followed by cells (2,000 cells/well) in 5µl STIM. STIM buffer consisted of Hanks Balanced Salt Solution supplemented with 0.1% BSA, 20 mM HEPES, 500 µM IBMX, and 100 µM ascorbic acid. The final DMSO concentration was 1.8%. To reduce likelihood of precipitation, test compounds remained in DMSO until the penultimate dilution into 50% of the final assay volume.

Downloaded from molpharm.aspetjournals.org at ASPET Journals on April 20, 2024

Molecular Pharmacology Fast Forward. Published on December 12, 2022 as DOI: 10.1124/molpharm.122.000605
This article has not been copyedited and formatted. The final version may differ from this version.

In both versions of the assay, plates were incubated at room temperature for a total reaction time of 60 min. Cyclic AMP production was quantified using homogeneous time-resolved fluorescence (HTRF) detection (Cisbio, Bedford, MA) according to vendor instructions: lysis buffer containing anti-cAMP cryptate (5 µl) and D2-conjugate (5 µl) was added to the wells, plates were incubated for an additional 60-90 min, and time-resolved fluorescence was detected using an EnVision plate reader (PerkinElmer).

Fluorescence data were converted to cAMP concentrations using a cAMP standard curve. For potentiator-mode concentration-response curves, results for each construct were expressed as percent of the window between an EC_{20} concentration of dopamine alone and the maximum response to dopamine in that construct. For the curve shift assays, concentration-response curves were expressed as percent of window between STIM buffer alone and 8 uM of dopamine.

Curve-fitting analysis. Cyclic AMP values were fit to a four-parameter logistic equation with equal weighting using GraphPad version 9.3.1 (San Diego, CA, USA).

The allosteric activity of a PAM is characterized by two experimentally-derived parameters: α denotes the leftward shift of the agonist CRC, defined as the ratio between the EC_{50} for agonist alone and the EC_{50} for agonist in the presence of one or more PAMs (EC_{50}/EC_{50}' ratio), while β denotes the increase in maximum efficacy for agonist elicited by one or more PAMs. The overall allosteric boost is defined as $\gamma = \alpha \cdot \beta$. In the present study, β was about 1.1 (see Fig. 4, below), indicating that dopamine was nearly a full agonist in this system. In contrast, α-shifts for the three PAMs separately and in combination spanned up to three orders of magnitude. Given that β contributed only about 1% of the maximum allosteric boost (0.04 log units for β, compared to 3 log units for α), further analysis focused on α.

Downloaded from molpharm.aspetjournals.org at ASPET Journals on April 20, 2024

Molecular Pharmacology Fast Forward. Published on December 12, 2022 as DOI: 10.1124/molpharm.122.000605
This article has not been copyedited and formatted. The final version may differ from this version.

For α-shift analysis (Figs. 5 and 7, below), EC_{50}/EC_{50}' ratios were calculated separately for each day's experiment, and the experiments were then combined and fit to the equation

$$y = \text{bottom} + \text{span} \cdot x / (K_B + x),$$

where y is α-shift for dopamine, x is the concentration of PAM A varied in CRC, K_B is the half-maximal concentration for PAM A, bottom is the α-shift for PAM B (or B + C) at fixed concentration, top is the maximum α-shift, and span is top minus bottom. Weighting was set to the inverse square of the Y-value (α-shift). For a single PAM, the bottom is fixed to 1 and the equation is mathematically equivalent to Equation 25 of (Ehlert, 1988) except that the variable names have been changed to GraphPad usage. In the case of a CRC for PAM A in the presence of fixed PAM B, bottom is the α-shift for B alone and top is the maximum α-shift for both PAMs combined. It should be noted that this method of analysis is the same as the Schild analysis customarily used for competitive antagonists and NAMs except that here α denotes a leftward shift.

Standard error values for fitted parameters were computed in GraphPad as previously described (Wang et al., 2018). The SE of the log EC_{50} provided by GraphPad was converted to SE of the untransformed (linear) EC_{50} by the e*q*uation:

$$SE_{linear} = \ln(10) \bullet EC_{50} \bullet SE_{log}$$

Downloaded from molpharm.aspetjournals.org at ASPET Journals on April 20, 2024

Molecular Pharmacology Fast Forward. Published on December 12, 2022 as DOI: 10.1124/molpharm.122.000605
This article has not been copyedited and formatted. The final version may differ from this version.

RESULTS

Characterization of the enantiomers of Compound A. In the initial publication (Lewis et al., 2015), Compound A was a racemic mixture of the two enantiomers with *anti* relative stereochemistry between the cyclopropyl and piperazine groups. We resynthesized Compound A (Supplemental Data II: Synthesis of BMS-A1 and Stereoisomers), separated the two enantiomers, and found that one enantiomer was roughly 3-fold more potent than the other (EC_{50} values 1,240 ± 130 nM vs 3,500 ± 300, Table S1). [The two *syn* isomers were also synthesized and were found to be less potent (EC_{50} values 6,100 and 7,300 nM).] The fairly similar activity of the four isomers suggests a rather loose fit with the D1 receptor, which is also consistent with their modest affinity values relative to the size of the molecule. The more-active enantiomer, henceforth referred to as BMS-A1, was utilized for all subsequent studies.

Identification of the general binding region (quadrant) for BMS-A1 using D1/D5 chimeras. BMS-A1 was tested in four D1/D5 chimeras that were previously used to characterize the binding sites for DETQ and MLS6585. In each of these, half of the D1 receptor (N-terminal versus C-terminal or extracellular versus intracellular) was replaced with its D5 counterpart (Wang et al., 2018). The combined results for the four chimeras identify which quadrant of the receptor is required for PAM activity; for instance, DETQ is only active when the N-terminal and intracellular halves are D1, implying that it binds to the N-terminal/intracellular quadrant. In wild-type D1 receptor, BMS-A1 potentiated the dopamine response with an EC_{50} of 3.4 μM and a maximum response that was 117% of the dopamine maximum (Fig. 2 and Table 1). This is in reasonable agreement with published results for the racemic mixture (Lewis et al., 2015). In contrast, BMS-A1 antagonized the dopamine response in the wild-type D5 receptor. [We did not further characterize whether the antagonism was orthosteric, allosteric, or nonspecific.]

Downloaded from molpharm.aspetjournals.org at ASPET Journals on April 20, 2024

Molecular Pharmacology Fast Forward. Published on December 12, 2022 as DOI: 10.1124/molpharm.122.000605
This article has not been copyedited and formatted. The final version may differ from this version.

Replacing either the extracellular or N-terminal half of the D1 receptor with its D5 counterpart abolished PAM activity, whereas replacing the cytoplasmic or C-terminal half with D5 left PAM activity unchanged. These results indicate that BMS-A1 binds to the N-terminal/extracellular quadrant of the D1 receptor ("upper left" quadrant in the standard orientation for depiction of GPCRs). BMS-A1 thus occupies a unique third allosteric site, setting it apart from DETQ (lower left quadrant) and MLS6585 (upper right quadrant) (Wang et al., 2018; Luderman et al., 2021).

Mutual synergy between three D1 PAMs in the absence of dopamine. If two molecules stabilize the same protein conformation but act at different sites, their free energies of binding should be additive, implying that their effects on the conformational equilibrium should be multiplicative (synergistic). Since agonists and PAMs both work by selectively binding to the active state of a given receptor (Bruns and Fergus, 1990; Ehlert and Griffin, 2014), a PAM + PAM combination should show the same qualitative synergy as a PAM + agonist combination, as long as the two PAMs bind to independent sites. In agreement with this prediction, DETQ and MLS6585 have been shown to interact multiplicatively in the absence of dopamine (Wang et al., 2018). In the case of three independent PAM sites, each pairwise combination as well as the triple combination should show synergy. This prediction provides a confirmatory test of the independence of the three sites.

In the current series of experiments, the limit of detection for an increase in cAMP was about 1% of the maximum response to dopamine. MLS6585 and BMS-A1 showed very small but detectable allo-agonist activity: 1.2% ± 0.1 for 80 μM MLS6585 and 2.0% ± 0.5 for 80 μM BMS-A1 (see bottom values for DETQ curves in Table S2). The allo-agonist response (if any) to DETQ was below the detection limit. Previously (Svensson et al., 2017), DETQ was reported to show variable allo-agonist activity, ranging from 2.7% to 13% (n=4). The prior study used the

Downloaded from molpharm.aspetjournals.org at ASPET Journals on April 20, 2024

Molecular Pharmacology Fast Forward. Published on December 12, 2022 as DOI: 10.1124/molpharm.122.000605
This article has not been copyedited and formatted. The final version may differ from this version.

same cell line but was conducted about 8 years before the current experiments; the difference may be due to minor variations in experimental protocol.

Each pairwise PAM combination showed much greater cAMP accumulation than the sum of each PAM separately (Fig. 3 and Table S2). For DETQ + MLS6585, maximum cAMP was 4.7% of the dopamine maximum, compared to <1% and 1.2% separately; for DETQ + BMS-A1, 15.2% compared to <1% and 2.0%; and for MLS6585 + BMS-A1, 26.6% compared to 1.2% and 2.0%. All three pairwise combinations showed synergy, implying that the three PAMs bind to different sites but stabilize the same active conformation or conformations. Further supporting this conclusion, the triple combination showed an additional supra-additive interaction, reaching 63.8% of the dopamine maximum.

Hill coefficients for BMS-A1 in this experiment were noticeably higher than unity, typically about 2 (see Fig. 3 panels B and C and Table S2).

Multiplicative leftward shift of the dopamine CRC by combinations of two PAMs. From receptor theory, the mutual synergy between two PAMs in the absence of dopamine should also cause a larger leftward shift in the dopamine CRC compared to either PAM separately. In other words, the three free energies (PAM A, PAM B, and agonist) should be additive, resulting in multiplicative effects on affinity. This has been confirmed for the combination of MLS6585 with ICL2 binders (Luderman et al., 2018). Assuming that BMS-A1 activates the same receptor conformation, it should show a similar supra-additive response with either DETQ or MLS6585 separately and possibly also in a triple combination with both PAMs.

In agreement with this prediction, BMS-A1 caused a marked increase in the ability of DETQ to elicit a leftward shift (α-shift) in the dopamine CRC (Fig. 4, middle column), increasing the α-shift from 18-fold for DETQ alone to about 200-fold for the combination (Fig. 5, panel B; see Table 2

Downloaded from molpharm.aspetjournals.org at ASPET Journals on April 20, 2024

Molecular Pharmacology Fast Forward. Published on December 12, 2022 as DOI: 10.1124/molpharm.122.000605
This article has not been copyedited and formatted. The final version may differ from this version.

for best-fit parameters). A similar multiplicative interaction was observed between BMS-A1 and MLS6585 (Fig. 4, right column), in which MLS6585 increased the α-shift for BMS-A1 from about 100-fold to roughly 500-fold (Fig. 5, panel C). [The CRCs for BMS-A1 began to curve down at the highest concentrations but did not achieve well-defined plateau values; because of this, the best-fit values for K_B and maximum α-shift were poorly characterized due to high correlation between the two parameters, but the initial slopes of the curves were still well-defined (Table 2).] Finally, the expected synergy between DETQ and MLS6585 was confirmed (Fig. 4, left column, Fig. 5 panel A). Each of these interactions was concentration-dependent (Fig. 5).

The maximum response to dopamine was barely increased by the PAMs, either singly or in combination (Fig. 4), with β (fold increase in the maximum response to agonist) usually 1.1 or less. Dopamine is therefore nearly a completely full agonist (efficacy >90%) and overall allosteric enhancement, defined as $\gamma = \alpha \cdot \beta$ (Ehlert and Griffin, 2014), is almost completely dominated by α.

It should be noted that the 10 and 20 μM concentrations of BMS-A1 lowered the maximum response to dopamine (Fig. 4, right column) while still affording a small additional leftward shift of the dopamine EC_{50} (Fig. 5, panel C), suggesting nonspecific inhibition of cAMP accumulation at these higher concentrations.

Triple combination. The combination of all three PAMs caused an additional leftward shift in the CRC for dopamine (Fig. 6), with a maximum shift of 996-fold (Fig. 7 and Table 3). The interactions were separately concentration-dependent for each of the three PAMs (Fig. 7).

Leftward shifts from combinations of PAMs were much greater than additive, but were consistently slightly less than would be expected from a strictly multiplicative interaction (Fig. 8). For instance, DETQ caused an 18-fold leftward shift by itself, but its incremental shift was 10-

Downloaded from molpharm.aspetjournals.org at ASPET Journals on April 20, 2024

Molecular Pharmacology Fast Forward. Published on December 12, 2022 as DOI: 10.1124/molpharm.122.000605
This article has not been copyedited and formatted. The final version may differ from this version.

fold in the presence of 5 μM MLS6585, 8-fold in the presence of 5 μM BMS-A1, and 5-fold in the presence of both PAMs. A similar pattern was seen for MLS6585 and BMS-A1. In each case, the lowest incremental α-shift was seen when both of the other two PAMs were present.

Downloaded from molpharm.aspetjournals.org at ASPET Journals on April 20, 2024

Molecular Pharmacology Fast Forward. Published on December 12, 2022 as DOI: 10.1124/molpharm.122.000605
This article has not been copyedited and formatted. The final version may differ from this version.

DISCUSSION

The most important findings of this study are 1) the identification of a third allosteric site on the dopamine D1 receptor; and 2) the observation that D1 PAMs that act at different sites interact synergistically with each other as well as with dopamine.

Previously, various D1 PAMs, exemplified by DETQ, were shown to bind to intracellular loop 2 (Lewis et al., 2015; Luderman et al., 2018; Wang et al., 2018). A structurally different series of D1 PAMs, exemplified by MLS6585, was shown to bind to another site and to interact cooperatively with the ICL2 binders (Luderman et al., 2018; Wang et al., 2018). This site, which has not yet been characterized in detail, appears to be located in the C-terminal/extracellular quadrant of the D1 receptor (Luderman et al., 2021). Another D1 PAM, Compound A, was shown not to bind to ICL2 but its site of action was not further delineated (Lewis et al., 2015). The unique structure of Compound A led us to speculate that it could bind to a different site from other published D1 PAMs. We therefore synthesized BMS-A1, the more active enantiomer of Compound A, and characterized its binding location and its interaction with other D1 PAMs. We found that BMS-A1 binds to the N-terminal/extracellular quadrant of the dopamine D1 receptor, a location that is distinct from the two previously described D1 PAM sites. In addition, we found that BMS-A1 interacts multiplicatively with PAMs that bind to the other two sites, indicating that all three classes of PAMs stabilize the same active conformation (or population of conformations) of the D1 receptor.

A simple thermodynamic model of allosterism. According to the theory of linked equilibria (Monod et al., 1965), proteins that are under allosteric control can transition between two conformations, an inactive and an active state. Any ligand that binds selectively to one of the two conformations will drive the equilibrium in the direction of the corresponding state. PAMs bind to the active state, favoring activation, and NAMs bind to the inactive state, suppressing activity (Ehlert and Griffin, 2014). An interesting consequence occurs when two ligands bind

Downloaded from molpharm.aspetjournals.org at ASPET Journals on April 20, 2024

Molecular Pharmacology Fast Forward. Published on December 12, 2022 as DOI: 10.1124/molpharm.122.000605
This article has not been copyedited and formatted. The final version may differ from this version.

selectively to the same active conformation but at different sites: their free energies will be additive, which implies that their functional effects will be multiplicative, up to some saturation point. PAMs potentiate agonists (and vice versa) in this way. Importantly, in the simple two-state model, the active-state conformation is the same regardless of how the receptor is occupied, whether by agonist, allosteric modulator or modulators, or any combination of agonist and modulators (Ehlert, 2016). Output is determined solely by the fraction of receptors in the active state. The current study provides experimental results that can be used to test this model. The D1 PAMs appear to be particularly useful for this purpose because they appear to lack more complicated types of activity such as effector bias, probe dependence, or a required order of binding (Svensson et al., 2017; Luderman et al., 2018).

Diversity of GPCR allosteric sites. The identification of a third allosteric site on the D1 receptor brings home the point that any location that changes its conformation between the active and inactive conformations has the potential to host a ligand that distinguishes between these conformations. Such a ligand will be a PAM or NAM, depending on the direction of its selectivity. Given that much of the surface of a typical GPCR will shift in the transition between active and inactive states (Rasmussen et al., 2011), this provides considerable scope for discovery of different allosteric sites, and multiple such sites have been reported for GPCRs (Thal et al., 2018; Wang et al., 2021). The exact location of the binding site for BMS-A1 requires further delineation, but the N-terminal/extracellular quadrant is known to host allosteric modulators for GPR40, P2Y1, and PAR2 (Thal et al., 2018). This general location is also the site of a cleft or tunnel through which several lipid mediators enter the orthosteric sites of their respective GPCRs (Hanson et al., 2012). The adenosine A_1 PAM series has been localized by cryo electron microscopy to the extracellular sections of transmembrane helices 1,6, and 7 (Draper-Joyce et al., 2021), and thus could overlap with the binding sites for BMS-A1 or MLS6585, or both. The A_1 PAM series bears some structural resemblance in its core scaffold to

Downloaded from molpharm.aspetjournals.org at ASPET Journals on April 20, 2024

Molecular Pharmacology Fast Forward. Published on December 12, 2022 as DOI: 10.1124/molpharm.122.000605
This article has not been copyedited and formatted. The final version may differ from this version.

MLS6585. Somewhat oddly, none of the three D1 PAMs binds to the vestibule region (ECL2, ECL3, and nearby transmembrane segments), which is a well-known hotspot for muscarinic NAMs and PAMs (Kruse et al., 2013). However, unlike the five muscarinic receptors, the D1 and D5 receptors show poor conservation of ECL2, suggesting disordered structure (https://www.uniprot.org).

Reciprocity of PAM and agonist. Although PAMs and orthosteric agonists at first glance would appear to possess qualitatively different types of activity, the two-state model indicates that both operate by selectively binding to the activated state, the only difference being the binding location. The apparent qualitative difference is undoubtedly due to the shaping of the agonist/receptor interaction by millions of years of evolution, resulting in much higher active-state affinity and selectivity for endogenous agonists compared to PAMs, which are generally discovered by screening and optimized by (at most) a few years of medicinal chemistry. Although PAMs are thought of as potentiators for agonists, the reverse interpretation is equally valid, as seen by the ability of agonists to enhance the binding of PAMs (Gavish and Snyder, 1980). The parallelism between agonists and PAMs leads to the prediction that PAMs should have some degree of efficacy on their own (allo-agonism), which was observed already in the first GPCR PAMs (Bruns and Fergus, 1990). Furthermore, provided they act at different sites, PAMs should potentiate each other, and the current study confirms this prediction in each of the possible 2- and 3-way combinations (Fig. 3).

Saturation of multiplicative leftward shift. The two-state model predicts that multiplicative interactions should begin to wane when a large fraction of the receptor population is already in the active state. Such a ceiling effect is seen for the triple PAM combination (Fig. 8). Can we use these results to estimate the fraction of D1 receptors in the active state under basal conditions? The 1,000-fold α-shift observed with the triple combination (Fig. 7) indicates that this PAM combination increases the active-state population by 1,000-fold, which in turn implies

Downloaded from molpharm.aspetjournals.org at ASPET Journals on April 20, 2024

Molecular Pharmacology Fast Forward. Published on December 12, 2022 as DOI: 10.1124/molpharm.122.000605
This article has not been copyedited and formatted. The final version may differ from this version.

that less than 1/1000th of the receptor is constitutively active. At the same time, the increase in dopamine affinity for the triple combination lags behind the roughly 4,000-fold shift expected from multiplying the three single α-shifts, indicating that this combination is beginning to approach a limit that presumably represents full occupation of the active state. The maximum α-shift is consistent with an inactive:active-state ratio (ε_0) of around 1,600 under basal conditions, although this estimated value has a wide confidence interval and is almost entirely dependent on a single data point (Table 4 and Fig. 9). Nevertheless, the same combination (2 μM DETQ + 5 μM MLS6585 + 5 μM BMS-A1) caused a 63.8% allo-agonist response in the absence of dopamine (Fig. 3), again suggesting that this combination approaches but does not reach full occupation of the active state. Overall, the results provide a tentative demonstration that PAM combinations can be used to probe relative levels of active and inactive receptor states.

We also constructed a chemical equilibrium-based model for the four-ligand interaction with the D1 receptor (Supplemental Data I: Four-Site Allosteric Model), and predictions from this model were qualitatively consistent with the experimental data.

Limitations and advantages of D1 PAMs as pharmacological tools. The CRC for BMS-A1 shows a downward slope at higher concentrations beginning around 10-20 μM (Fig 4, right column). This phenomenon is also seen with DETQ and MLS6585 at about the same concentrations (data not shown). It does not appear to be due to activity at the D1 receptor, because DETQ is much more potent than the other two compounds in PAM activity but about the same as the others in this inhibitory effect. It may involve inhibition of cAMP generation.by a non-specific mechanism associated with hydrophobic compounds, such as formation of aggregates (Irwin et al., 2015). Because of this inhibition, it is difficult to measure the true maximum α-shifts for MLS6585 and BMS-A1. On the other hand, DETQ reaches a plateau before the onset of this downward effect, so its roughly 20-fold maximum α-shift is probably a

Downloaded from molpharm.aspetjournals.org at ASPET Journals on April 20, 2024

Molecular Pharmacology Fast Forward. Published on December 12, 2022 as DOI: 10.1124/molpharm.122.000605
This article has not been copyedited and formatted. The final version may differ from this version.

true measure of its selectivity for the active form over the inactive form of the D1 receptor. More potent analogs of MLS6585 and BMS-A1 would be useful.

Conversely, the D1 PAMs may be useful tools for studying the two-state model because they lack more complicated pharmacology seen with other PAMs. In particular, DETQ and MLS6585 appear to lack biased signaling and probe dependence (Svensson et al., 2017; Luderman et al., 2018). In addition, the three D1 PAMs do not bind to the vestibule region and therefore are unlikely to impede access of ligands to the orthosteric binding pocket. Finally, the availability of PAMs acting at three independent sites on the D1 receptor affords a unique opportunity to investigate various phenomena predicted by the two state model, such as multiplicative effects between PAMs and between PAMs and agonists.

Therapeutic possibilities. PAMs amplify physiological control circuits, and the potential therapeutic advantages of this approach have long been known (Bruns and Fergus, 1990; Nemeth et al., 1998; Christopoulos and Kenakin, 2002). In the D1 system in particular, the PAM mevidalen, a close analog of DETQ, has shown efficacy versus both motor and non-motor symptoms of patients with Lewy Body Dementia and Parkinson's disease (Biglan et al., 2022).

Going further, combinations of allosteric modulators may have advantages over single agents. For instance, two PAMs that acted at different sites could be effective at much lower doses than either dosed separately, potentially circumventing pharmacokinetic limitations or non-mechanism-related toxicity. Greater efficacy might also be obtained from a greater maximum α-shift of the combination or from greater allo-agonism in situations where the endogenous agonist is not present. Conversely, our results are a reminder that synergistic combinations (agonist + PAM or PAM + PAM) carry the risk of therapeutic overshoot.

Biased signaling involves the presence of two different active conformations, each related to a different downstream effector pathway (Kenakin and Christopoulos, 2013). In theory,

Downloaded from molpharm.aspetjournals.org at ASPET Journals on April 20, 2024

Molecular Pharmacology Fast Forward. Published on December 12, 2022 as DOI: 10.1124/molpharm.122.000605
This article has not been copyedited and formatted. The final version may differ from this version.

compounds showing biased signaling could have a superior margin of safety, but designing drugs with a clinically significant degree of signal bias has proven to be difficult. The thermodynamic model, when extended to two active conformations, predicts that signaling bias should be multiplicative, which could allow two drugs each with a modest degree of bias (agonist + PAM, or two PAMs acting at independent sites) to together produce a more robust degree of bias.

Combinations of NAMs acting at independent sites could also have advantages. A single NAM has a maximum rightward shift determined by its selectivity for the inactive state. With two NAMs acting at different sites, rightward shifts would multiply, allowing lower dosing and/or a larger maximum effect. In addition, if two NAMs acting at different sites each separately showed therapeutic activity, treatment with the combination might make it less likely for a single mutation to cause resistance, which could be advantageous in treating disorders such as cancer (Hany et al., 2022) and infectious disease (Naidu et al., 2022) in which the appearance of resistance can abrogate the effectiveness of a treatment.

Basis for discovery of allosteric drugs. In conclusion, our results re-emphasize two points, both known from theory but not so often exemplified experimentally. First, whenever a protein is under allosteric control, it must exist in at least two conformations. Any part of the protein that changes its shape between these conformations can potentially host a molecule that binds selectively to one of these conformations, allosterically modifying the protein's function. This presents opportunities for discovery of allosteric drugs. In the current study, we describe four such sites on the dopamine D1 receptor: the orthosteric site for dopamine and three independent sites for allosteric modulators. Second, whenever two or more ligands bind selectively to the same protein conformation, their free energies are additive, hence their functional effects are multiplicative. This presents opportunities for combinatorial effects on

Downloaded from molpharm.aspetjournals.org at ASPET Journals on April 20, 2024

Molecular Pharmacology Fast Forward. Published on December 12, 2022 as DOI: 10.1124/molpharm.122.000605
This article has not been copyedited and formatted. The final version may differ from this version.

physiology. In the current study, we describe up to 1,000-fold amplification of the potency of dopamine by combinations of three allosteric modulators.

Downloaded from molpharm.aspetjournals.org at ASPET Journals on April 20, 2024

Molecular Pharmacology Fast Forward. Published on December 12, 2022 as DOI: 10.1124/molpharm.122.000605
This article has not been copyedited and formatted. The final version may differ from this version.

AUTHORSHIP CONTRIBUTIONS

Participated in research design: Wang, Goldsmith, Svensson, Willard, Bruns

Conducted experiments: Wang, Goldsmith

Contributed new reagents or analytic tools: Goldsmith, Beck

Performed data analysis: Wang, Hembre, Goldsmith, Willard, Bruns

Wrote or contributed to the writing of the manuscript: Wang, Hembre, Goldsmith, Svensson, Willard, Bruns

Downloaded from molpharm.aspetjournals.org at ASPET Journals on April 20, 2024

Molecular Pharmacology Fast Forward. Published on December 12, 2022 as DOI: 10.1124/molpharm.122.000605
This article has not been copyedited and formatted. The final version may differ from this version.

REFERENCES

Alexander SP, Christopoulos A, Davenport AP, Kelly E, Mathie A, Peters JA, Veale EL, Armstrong JF, Faccenda E, Harding SD, Pawson AJ, Southan C, Davies JA, Abbracchio MP, Alexander W, Al-Hosaini K, Back M, Barnes NM, Bathgate R, Beaulieu JM, Bernstein KE, Bettler B, Birdsall NJM, Blaho V, Boulay F, Bousquet C, Brauner-Osborne H, Burnstock G, Calo G, Castano JP, Catt KJ, Ceruti S, Chazot P, Chiang N, Chini B, Chun J, Cianciulli A, Civelli O, Clapp LH, Couture R, Csaba Z, Dahlgren C, Dent G, Singh KD, Douglas SD, Dournaud P, Eguchi S, Escher E, Filardo EJ, Fong T, Fumagalli M, Gainetdinov RR, Gasparo M, Gerard C, Gershengorn M, Gobeil F, Goodfriend TL, Goudet C, Gregory KJ, Gundlach AL, Hamann J, Hanson J, Hauger RL, Hay DL, Heinemann A, Hollenberg MD, Holliday ND, Horiuchi M, Hoyer D, Hunyady L, Husain A, AP IJ, Inagami T, Jacobson KA, Jensen RT, Jockers R, Jonnalagadda D, Karnik S, Kaupmann K, Kemp J, Kennedy C, Kihara Y, Kitazawa T, Kozielewicz P, Kreienkamp HJ, Kukkonen JP, Langenhan T, Leach K, Lecca D, Lee JD, Leeman SE, Leprince J, Li XX, Williams TL, Lolait SJ, Lupp A, Macrae R, Maguire J, Mazella J, McArdle CA, et al. (2021) THE CONCISE GUIDE TO PHARMACOLOGY 2021/22: G protein-coupled receptors. *Br J Pharmacol* **178 Suppl 1**:S27-S156.

Arnsten AF, Girgis RR, Gray DL and Mailman RB (2017) Novel Dopamine Therapeutics for Cognitive Deficits in Schizophrenia. *Biol Psychiatry* **81**:67-77.

Beadle CD, Coates DA, Hao J, Krushinski JH, Reinhard MR, Schaus JM and Wolfangel CD (2014) 3,4-dihydroisoquinolin-2(1H)-yl compounds WO 2014/193781 A1, in pp 1-90.

Beaulieu JM and Gainetdinov RR (2011) The physiology, signaling, and pharmacology of dopamine receptors. *Pharmacol Rev* **63**:182-217.

Downloaded from molpharm.aspetjournals.org at ASPET Journals on April 20, 2024

Molecular Pharmacology Fast Forward. Published on December 12, 2022 as DOI: 10.1124/molpharm.122.000605
This article has not been copyedited and formatted. The final version may differ from this version.

Biglan K, Munsie L, Svensson KA, Ardayfio P, Pugh M, Sims J and Brys M (2022) Safety and Efficacy of Mevidalen in Lewy Body Dementia: A Phase 2, Randomized, Placebo‐Controlled Trial. *Movement Disorders* **37**:513-524.

Bruns RF and Fergus JH (1990) Allosteric enhancement of adenosine A1 receptor binding and function by 2-amino-3-benzoylthiophenes. *Mol Pharmacol* **38**:939-949.

Bruns RF, Mitchell SN, Wafford KA, Harper AJ, Shanks EA, Carter G, O'Neill MJ, Murray TK, Eastwood BJ, Schaus JM, Beck JP, Hao J, Witkin JM, Li X, Chernet E, Katner JS, Wang H, Ryder JW, Masquelin ME, Thompson LK, Love PL, Maren DL, Falcone JF, Menezes MM, Zhang L, Yang CR and Svensson KA (2018) Preclinical profile of a dopamine D1 potentiator suggests therapeutic utility in neurological and psychiatric disorders. *Neuropharmacology* **128**:351-365.

Christopoulos A and Kenakin T (2002) G protein-coupled receptor allosterism and complexing. *Phamacol Rev* **54**:323-374.

Draper-Joyce CJ, Bhola R, Wang J, Bhattarai A, Nguyen AT, O'Sullivan K, Chia LY, Venugopal H, Valant C and Thal DM (2021) Positive allosteric mechanisms of adenosine A1 receptor-mediated analgesia. *Nature* **597**:571-576.

Ehlert F and Griffin M (2014) Estimation of Ligand Affinity Constants for Receptor States in Functional Studies Involving the Allosteric Modulation of G Protein-Coupled Receptors: Implications for Ligand Bias. *Journal of pharmacological and toxicological methods* **69**:253-279.

Ehlert FJ (1988) Estimation of the affinities of allosteric ligands using radioligand binding and pharmacological null methods. *Mol Pharmacol* **33**:187-194.

Ehlert FJ (2016) Cooperativity Has Empirical and Ultimate Levels of Explanation. *Trends in Pharmacological Sciences* **37**:620-623.

Downloaded from molpharm.aspetjournals.org at ASPET Journals on April 20, 2024

Molecular Pharmacology Fast Forward. Published on December 12, 2022 as DOI: 10.1124/molpharm.122.000605
This article has not been copyedited and formatted. The final version may differ from this version.

Felsing DE, Jain MK and Allen JA (2019) Advances in Dopamine D1 Receptor Ligands for Neurotherapeutics. *Curr Top Med Chem* **19**:1365-1380.

Gavish M and Snyder SH (1980) Benzodiazepine recognition sites on GABA receptors. *Nature* **287**:651-652.

Hanson MA, Roth CB, Jo E, Griffith MT, Scott FL, Reinhart G, Desale H, Clemons B, Cahalan SM, Schuerer SC, Sanna MG, Han GW, Kuhn P, Rosen H and Stevens RC (2012) Crystal Structure of a Lipid G Protein-Coupled Receptor. *Science* **335**:851-855.

Hany R, Leyris J-P, Bret G, Mallié S, Sar C, Thouaye M, Hamze A, Provot O, Sokoloff P, Valmier J, Villa P and Rognan D (2022) High-Throughput Screening for Extracellular Inhibitors of the FLT3 Receptor Tyrosine Kinase Reveals Chemically Diverse and Druggable Negative Allosteric Modulators. *ACS Chemical Biology* **17**:709-722.

Hao J, Beck JP, Schaus JM, Krushinski JH, Chen Q, Beadle CD, Vidal P, Reinhard MR, Dressman BA, Massey SM, Boulet SL, Cohen MP, Watson BM, Tupper D, Gardinier KM, Myers J, Johansson AM, Richardson J, Richards DS, Hembre EJ, Remick DM, Coates DA, Bhardwaj RM, Diseroad BA, Bender D, Stephenson G, Wolfangel CD, Diaz N, Getman BG, Wang X-s, Heinz BA, Cramer JW, Zhou X, Maren DL, Falcone JF, Wright RA, Mitchell SN, Carter G, Yang CR, Bruns RF and Svensson KA (2019) Synthesis and Pharmacological Characterization of 2-(2,6-Dichlorophenyl)-1-((1S,3R)-5-(3-hydroxy-3-methylbutyl)-3-(hydroxymethyl)-1-methyl-3,4-dihydroisoquinolin-2(1H)-yl)ethan-1-one (LY3154207), a Potent, Subtype Selective, and Orally Available Positive Allosteric Modulator of the Human Dopamine D1 Receptor. *Journal of Medicinal Chemistry* **62**:8711-8732.

Ikemoto S, Glazier BS, Murphy JM and McBride WJ (1997) Role of dopamine D1 and D2 receptors in the nucleus accumbens in mediating reward. *J Neurosci* **17**:8580-8587.

Downloaded from molpharm.aspetjournals.org at ASPET Journals on April 20, 2024

Molecular Pharmacology Fast Forward. Published on December 12, 2022 as DOI: 10.1124/molpharm.122.000605
This article has not been copyedited and formatted. The final version may differ from this version.

Irwin JJ, Duan D, Torosyan H, Doak AK, Ziebart KT, Sterling T, Tumanian G and Shoichet BK (2015) An Aggregation Advisor for Ligand Discovery. *Journal of Medicinal Chemistry* **58**:7076-7087.

Kenakin T and Christopoulos A (2013) Signalling bias in new drug discovery: detection, quantification and therapeutic impact. *Nat Rev Drug Discov* **12**:205-216.

Kenakin TP (2010) Ligand detection in the allosteric world. *J Biomol Screen* **15**:119-130.

Kruse AC, Ring AM, Manglik A, Hu J, Hu K, Eitel K, Hubner H, Pardon E, Valant C, Sexton PM, Christopoulos A, Felder CC, Gmeiner P, Steyaert J, Weis WI, Garcia KC, Wess J and Kobilka BK (2013) Activation and allosteric modulation of a muscarinic acetylcholine receptor. *Nature* **504**:101-106.

Lewis MA, Hunihan L, Watson J, Gentles RG, Hu S, Huang Y, Bronson J, Macor JE, Beno BR, Ferrante M, Hendricson A, Knox RJ, Molski TF, Kong Y, Cvijic ME, Rockwell KL, Weed MR, Cacace AM, Westphal RS, Alt A and Brown JM (2015) Discovery of D1 dopamine receptor positive allosteric modulators: characterization of pharmacology and identification of residues that regulate species selectivity. *J Pharmacol Exp Ther* **354**:340-349.

Luderman K, Free RB, Koenigsberg F, Aubé J, Frankowski K, Neve K and Sibley D (2021) Characterization of a D1 Dopamine Receptor Positive Allosteric Modulator with a Novel Binding Site. *The FASEB Journal* **35 S1**:2361.

Luderman KD, Conroy JL, Free RB, Southall N, Ferrer M, Sanchez-Soto M, Moritz AE, Willette BK, Fyfe TJ, Jain P, Titus S, Hazelwood LA, Aube J, lane JR, Frankowski KJ and Sibley DR (2018) Identification of positive allosteric modulators of the D1 dopamine receptor that act at diverse binding sites. *Molecular Pharmacology* **94**:1197-1209.

May LT, Leach K, Sexton PM and Christopoulos A (2007) Allosteric modulation of G protein-coupled receptors. *Annu Rev Pharmacol Toxicol* **47**:1-51.

Downloaded from molpharm.aspetjournals.org at ASPET Journals on April 20, 2024

Molecular Pharmacology Fast Forward. Published on December 12, 2022 as DOI: 10.1124/molpharm.122.000605
This article has not been copyedited and formatted. The final version may differ from this version.

Monod J, Wyman J and Changeux J-P (1965) On the nature of allosteric transitions: a plausible model. *J Mol Biol* **12**:88-118.

Naidu BN, Patel M, McAuliffe B, Ding B, Cianci C, Simmermacher J, Jenkins S, Parker DD, Sivaprakasam P, Khan JA, Kish K, Lewis H, Hanumegowda U, Krystal M, Meanwell NA and Kadow JF (2022) Design, Synthesis, and Preclinical Profiling of GSK3739936 (BMS-986180), an Allosteric Inhibitor of HIV-1 Integrase with Broad-Spectrum Activity toward 124/125 Polymorphs. *Journal of Medicinal Chemistry* **65**:4949-4971.

Nakamura T, Sato A, Kitsukawa T, Momiyama T, Yamamori T and Sasaoka T (2014) Distinct motor impairments of dopamine D1 and D2 receptor knockout mice revealed by three types of motor behavior. *Front Integr Neurosci* **8**:56.

Nemeth EF, Steffey ME, Hammerland LG, Hung BC, Van Wagenen BC, DelMar EG and Balandrin MF (1998) Calcimimetics with potent and selective activity on the parathyroid calcium receptor. *Proc Natl Acad Sci USA* **95**:4040-4045.

Rasmussen SG, Choi HJ, Fung JJ, Pardon E, Casarosa P, Chae PS, Devree BT, Rosenbaum DM, Thian FS, Kobilka TS, Schnapp A, Konetzki I, Sunahara RK, Gellman SH, Pautsch A, Steyaert J, Weis WI and Kobilka BK (2011) Structure of a nanobody-stabilized active state of the β2 adrenoceptor. *Nature* **469**:175-180.

Santos R, Ursu O, Gaulton A, Bento AP, Donadi RS, Bologa CG, Karlsson A, Al-Lazikani B, Hersey A, Oprea TI and Overington JP (2017) A comprehensive map of molecular drug targets. *Nat Rev Drug Discov* **16**:19-34.

Shiraki R, Tobe T, Kawakami S, Moritomo H and Ohmiya M (2015) Heterocyclic acetamide compound. *Patent Number: US20150045402A1*.

Stockton JM, Birdsall NJ, Burgen AS and Hulme EC (1983) Modification of the binding properties of muscarinic receptors by gallamine. *Mol Pharmacol* **23**:551-557.

Downloaded from molpharm.aspetjournals.org at ASPET Journals on April 20, 2024

Molecular Pharmacology Fast Forward. Published on December 12, 2022 as DOI: 10.1124/molpharm.122.000605
This article has not been copyedited and formatted. The final version may differ from this version.

Svensson KA, Hao J and Bruns RF (2019) Positive allosteric modulators of the dopamine D1 receptor: A new mechanism for the treatment of neuropsychiatric disorders. *Adv Pharmacol* **86**:273-305.

Svensson KA, Heinz BA, Schaus JM, Beck JP, Hao J, Krushinski JH, Reinhard MR, Cohen MP, Hellman SL, Getman BG, Wang X, Menezes MM, Maren DL, Falcone JF, Anderson WH, Wright RA, Morin SM, Knopp KL, Adams BL, Rogovoy B, Okun I, Suter TM, Statnick MA, Gehlert DR, Nelson DL, Lucaites VL, Emkey R, DeLapp NW, Wiernicki TR, Cramer JW, Yang CR and Bruns RF (2017) An allosteric potentiator of the dopamine D1 receptor increases locomotor activity in human D1 knock-in mice without causing stereotypy or tachyphylaxis. *J Pharmacol Exp Ther* **360**:117-128.

Teng X, Chen S, Nie Y, Xiao P, Yu X, Shao Z and Zheng S (2022) Ligand recognition and biased agonism of the D1 dopamine receptor. *Nature Communications* **13**:3186.

Thal DM, Glukhova A, Sexton PM and Christopoulos A (2018) Structural insights into G-protein-coupled receptor allostery. *Nature* **559**:45-53.

Wang X, Heinz BA, Qian Y-W, Carter JH, Gadski RA, Beavers LS, Little SP, Yang CR, Beck JP, Hao J, Schaus JM, Svensson KA and Bruns RF (2018) Intracellular binding site for a positive allosteric modulator of the dopamine D1 receptor. *Molecular Pharmacology* **94**:1232-1245.

Wang Y, Yu Z, Xiao W, Lu S and Zhang J (2021) Allosteric binding sites at the receptor–lipid bilayer interface: novel targets for GPCR drug discovery. *Drug Discovery Today* **26**:690-703.

Xiao P, Yan W, Gou L, Zhong Y-N, Kong L, Wu C, Wen X, Yuan Y, Cao S, Qu C, Yang X, Yang C-C, Xia A, Hu Z, Zhang Q, He Y-H, Zhang D-L, Zhang C, Hou G-H, Liu H, Zhu L, Fu P, Yang S, Rosenbaum DM, Sun J-P, Du Y, Zhang L, Yu X and Shao Z (2021) Ligand recognition and allosteric regulation of DRD1-Gs signaling complexes. *Cell* **184**:943-956.

Downloaded from molpharm.aspetjournals.org at ASPET Journals on April 20, 2024

Molecular Pharmacology Fast Forward. Published on December 12, 2022 as DOI: 10.1124/molpharm.122.000605
This article has not been copyedited and formatted. The final version may differ from this version.

Zhuang Y, Krumm B, Zhang H, Zhou XE, Wang Y, Huang X-P, Liu Y, Cheng X, Jiang Y and Jiang H (2021) Mechanism of dopamine binding and allosteric modulation of the human D1 dopamine receptor. *Cell research* **31**:593-596.

Downloaded from molpharm.aspetjournals.org at ASPET Journals on April 20, 2024

Molecular Pharmacology Fast Forward. Published on December 12, 2022 as DOI: 10.1124/molpharm.122.000605
This article has not been copyedited and formatted. The final version may differ from this version.

FOOTNOTES

This work was funded by Eli Lilly & Co. All authors are current or former employees of Eli Lilly & Co.

Downloaded from molpharm.aspetjournals.org at ASPET Journals on April 20, 2024

Molecular Pharmacology Fast Forward. Published on December 12, 2022 as DOI: 10.1124/molpharm.122.000605
This article has not been copyedited and formatted. The final version may differ from this version.

FIGURE LEGENDS

Fig. 1 Chemical Structures of D1 PAMs. Chemical Abstracts names: DETQ, [2-(2,6-dichlorophenyl)-1-((1S,3R)-3-(hydroxymethyl)-5-(2-hydroxypropan-2-yl)-1-methyl-3,4-dihydroisoquinolin-2(1H)-yl)ethan-1-one]; MLS6585, N-(6-(tert-butyl)-3-carbamoyl-4,5,6,7-tetrahydrobenzo[b]thiophen-2-yl)isonicotinamide; BMS-A1, [1-((rel-1S,3R,6R)-6-(benzo[d][1,3]dioxol-5-yl)bicyclo[4.1.0]heptan-3-yl)-4-(2-bromo-5-chlorobenzyl)piperazine]. The absolute configuration of BMS-A1 is unknown and could be either (1S,3R,6R) or (1R,3S,6S).

Fig. 2. Potentiation by BMS-A1 of the cAMP accumulation elicited by an EC_{20} concentration of dopamine in D1/D5 chimeras. The dopamine window is defined as the range between the cAMP response to an EC_{20} concentration of dopamine and the response to a maximum (8 μM) concentration of dopamine. The receptor diagram is taken (CC-BY) from (Wang et al., 2018). Abbreviations: CT (C-terminal); NT (N-terminal). The NT/CT breakpoint was at the extracellular end of TMH4, and the out/in breakpoints were at the midpoints of each transmembrane helix; see the Supplemental Data of (Wang et al., 2018) for the exact breakpoints. Values are means ± SE, n = 3. In the D5, $D5_{out}/D1_{in}$, and $D5_{NT}/D1_{CT}$ constructs, BMS-A1 inhibited cAMP accumulation. Although GraphPad was able to find best-fit values for the inhibitory curves, it was unable to compute confidence intervals for several fit parameters, and the curves are therefore included only as visual aids.

Fig. 3. Mutual potentiation of the allosteric agonist effects of DETQ, MLS6585, and BMS-A1 in the absence of dopamine. Values are means ± SE (n = 4 for panels A-C, n = 5 for panel D). Best-fit parameters for the curves are provided in Table S2.

Downloaded from molpharm.aspetjournals.org at ASPET Journals on April 20, 2024

Molecular Pharmacology Fast Forward. Published on December 12, 2022 as DOI: 10.1124/molpharm.122.000605
This article has not been copyedited and formatted. The final version may differ from this version.

Fig. 4. Potentiation of the cAMP response to dopamine by pairwise combinations of PAMs. In the left and middle columns, each curve represents a different concentration of DETQ; in the right column, each curve represents a different concentration of BMS-A1. Values are means of two replicates from a single experiment. The EC_{50} for dopamine alone was 55 ± 5 nM (n = 2). Composite best-fit α-shift values from this experiment and one other are given in Fig. 5, below.

Fig. 5. Leftward shift of concentration-response curves for dopamine in the presence of pairwise combinations of PAMs. EC_{50}/EC_{50}' (α-shift) is the control EC_{50} for dopamine divided by its EC_{50} in the presence of one or more PAMs. Values are means ± SE of α-shift values derived from two experiments. Curves are from a model in which top, bottom, and K_B are allowed to vary and the Hill coefficient is set to 1. See "Curve-fitting analysis" in Methods for a more detailed description. Best-fit parameters are provided in Table 2.

Fig. 6. Potentiation of the cAMP response to dopamine in the presence of two or three PAMs. Values are means of two replicates from a single experiment. Composite best-fit α-shift values from this experiment and two others are given in Fig. 7, below.

Fig. 7. Additional leftward shift for DETQ in the presence of one or both of the other two PAMs. EC_{50}/EC_{50}' (α-shift) is the control EC_{50} for dopamine divided by its EC_{50} in the presence of one or more PAMs. Values are means ± SE of α-shift values derived from three experiments, except for DETQ control curves (n = 2). Curves are from a model in which top, bottom, and K_B are allowed to vary and the Hill coefficient is set to 1. See "Curve-fitting analysis" in Methods for a more detailed description. Best-fit parameters are provided in Table 3.

Downloaded from molpharm.aspetjournals.org at ASPET Journals on April 20, 2024

Molecular Pharmacology Fast Forward. Published on December 12, 2022 as DOI: 10.1124/molpharm.122.000605
This article has not been copyedited and formatted. The final version may differ from this version.

Fig. 8. Diagram summarizing α-shift interactions. Absolute α-shift values are shown in blue at the vertices of the cube, and are taken from fitted bottoms and tops in Fig. 7a. Incremental shifts (in red) are shown at the edges of the cube. PAM concentrations are 5 μM for MLS6585 and BMS-A1; DETQ data are for CRCs up to 2 μM.

Fig. 9. Alpha-shifts predicted from multiplying single-PAM shifts, compared to experimentally observed α-shifts. Data are from Fig. 7 / Table 3 with additional data for 5 μM MLS6585 + 0.2 μM BMS-A1 (± DETQ) and the converse 0.2 μM + 5 μM combination. Data were fit to a 3-parameter CRC model with the bottom fixed to 1. The best-fit value for maximum observed α-shift was 1,610 (95% confidence interval 900 to 7.400); half-maximal observed shift occurred at a predicted shift of 1,710 (95% confidence interval 830 to 7,300).

Downloaded from molpharm.aspetjournals.org at ASPET Journals on April 20, 2024

Molecular Pharmacology Fast Forward. Published on December 12, 2022 as DOI: 10.1124/molpharm.122.000605
This article has not been copyedited and formatted. The final version may differ from this version.

Downloaded from molpharm.aspetjournals.org at ASPET Journals on April 20, 2024

Molecular Pharmacology Fast Forward. Published on December 12, 2022 as DOI: 10.1124/molpharm.122.000605
This article has not been copyedited and formatted. The final version may differ from this version.

TABLE 1.

Best-fit values for BMS-A1 CRCs in D1/D5 chimeras (data from Fig. 2).

Bottom and top values are expressed as percent of the dopamine window, defined as the difference between the maximum response to dopamine and the response to an EC_{20} concentration of dopamine. SE values of best-fit parameters were calculated as described in Methods.

	EC50 (nM)			Hill coefficient			bottom (%)			top (%)		
	mean		SE	mean		SE	mean		SE	mean		SE
D1	3400	±	400	1.22	±	0.14	1.87	±	1.72	117	±	4
D5	antagonist											
$D1_{out}/D5_{in}$	1760	±	180	1.55	±	0.21	2.7	±	1.9	102	±	3
$D5_{out}/D1_{in}$	antagonist											
$D1_{NT}/D5_{CT}$	1560	±	250	1.57	±	0.34	2.9	±	3.6	118	±	5
$D5_{NT}/D1_{CT}$	antagonist											

Downloaded from molpharm.aspetjournals.org at ASPET Journals on April 20, 2024

Molecular Pharmacology Fast Forward. Published on December 12, 2022 as DOI: 10.1124/molpharm.122.000605
This article has not been copyedited and formatted. The final version may differ from this version.

Table 2. Best-fit parameters for leftward shifts of the dopamine CRC in the presence of pairwise combinations of PAMs (Fig. 5).

DETQ CRC

	K_B (nM)			α-shift bottom			α-shift top		
MLS6585 (nM)	mean		SE	mean		SE	mean		SE
10000	38	±	6	10.7	±	0.8	112.3	±	6.2
5000	51	±	4	9.0	±	0.3	110.1	±	3.3
2500	49	±	4	5.4	±	0.2	77.4	±	2.5
1250	57	±	6	3.2	±	0.2	49.7	±	2.0
625	54	±	5	2.2	±	0.1	34.7	±	1.3
0	57	±	6	1.0	±	0.1	18.3	±	0.7

DETQ CRC

	K_B (nM)			α-shift bottom			α-shift top		
BMS-A1 (nM)	mean		SE	mean		SE	mean		SE
10000	11	±	3	19.2	±	3.0	164.1	±	11.2
5000	28	±	6	18.9	±	2.1	222.1	±	15.3
2500	48	±	5	10.2	±	0.5	170.5	±	6.8
1250	55	±	4	6.1	±	0.2	99.3	±	2.8
625	58	±	4	2.8	±	0.1	57.7	±	1.6
0	57	±	6	1.0	±	0.1	18.3	±	0.7

BMS-A1 CRC

	K_B (nM)			α-shift bottom			α-shift top		
MLS6585 (nM)	mean		SE	mean		SE	mean		SE
10000	5300	±	1400	12.4	±	1.0	513	±	87
5000	7500	±	1200	9.1	±	0.4	555	±	60
2500	13800	±	4300	5.5	±	0.4	603	±	143
1250	28400	±	11100	3.2	±	0.2	672	±	223
625	42700	±	21100	2.1	±	0.1	601	±	263
0	27500	±	8800	1.02	±	0.05	117	±	31

Downloaded from molpharm.aspetjournals.org at ASPET Journals on April 20, 2024

Molecular Pharmacology Fast Forward. Published on December 12, 2022 as DOI: 10.1124/molpharm.122.000605
This article has not been copyedited and formatted. The final version may differ from this version.

Table 3. Best-fit parameters for leftward shifts of the dopamine CRC in the presence of pairwise and triple combinations of PAMs (Fig. 7).

DETQ CRC

		K_B (nM)			α-shift bottom			α-shift top		
MLS6585 (μM)	BMS-A1 (μM)	mean		SE	mean		SE	mean		SE
0	0	57	±	6	1.0	±	0.1	18	±	1
5	0	43	±	4	9.6	±	0.4	105	±	4
0	5	54	±	10	24.5	±	2.0	297	±	21
5	5	12	±	3	195.9	±	18.1	996	±	50
1	0	48	±	4	2.9	±	0.1	43	±	1
0	1	51	±	5	4.5	±	0.3	88	±	4
1	1	52	±	6	19.4	±	1.1	295	±	13
0.2	0	58	±	5	1.3	±	0.1	24	±	1
0	0.2	60	±	7	1.7	±	0.1	30	±	1
0.2	0.2	59	±	6	2.2	±	0.1	41	±	2

Downloaded from molpharm.aspetjournals.org at ASPET Journals on April 20, 2024

Molecular Pharmacology Fast Forward. Published on December 12, 2022 as DOI: 10.1124/molpharm.122.000605
This article has not been copyedited and formatted. The final version may differ from this version.

Table 4. Comparison of values predicted from multiplying α-shifts from single PAMs with experimentally observed α-shifts for double and triple combinations.

	PAM			α-shift		
PAM combination	**DETQ (μM)**	**MLS6585 (μM)**	**BMS-A1 (μM)**	**predicted**	**observed**	**observed / predicted**
none	0	0	0	1	1	1
single	0	0.2	0	1.24	1.24	1
single	0	0	0.2	1.43	1.43	1
single	0	1	0	2.9	2.9	1
single	0	0	1	4.5	4.5	1
single	0	5	0	10	10	1
single	0	0	5	24	24	1
single	up to 2	0	0	18	18	1
double	0	5	5	240	196	0.82
double	up to 2	0.2	0	22	24	1.08
double	up to 2	0	0.2	26	30	1.15
double	up to 2	1	0	52	43	0.83
double	up to 2	0	1	81	88	1.08
double	up to 2	5	0	180	105	0.58
double	up to 2	0	5	432	297	0.69
triple	up to 2	0.2	0.2	32	39	1.22
triple	up to 2	1	1	232	295	1.27
triple	up to 2	5	0.2	257	225	0.88
triple	up to 2	0.2	5	536	483	0.90
triple	up to 2	5	5	4320	996	0.23

Downloaded from molpharm.aspetjournals.org at ASPET Journals on April 20, 2024

Molecular Pharmacology Fast Forward. Published on December 12, 2022 as DOI: 10.1124/molpharm.122.000605
This article has not been copyedited and formatted. The final version may differ from this version.

Downloaded from molpharm.aspetjournals.org at ASPET Journals on April 20, 2024

Figure 1

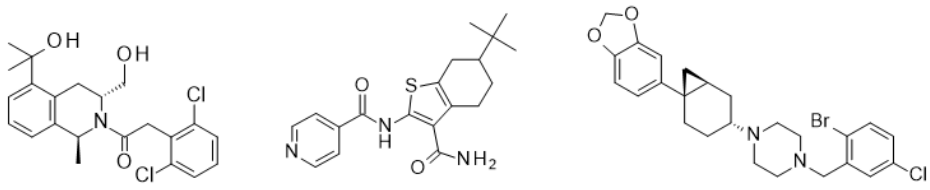

DETQ MLS6585 BMS-A1

Figure 2

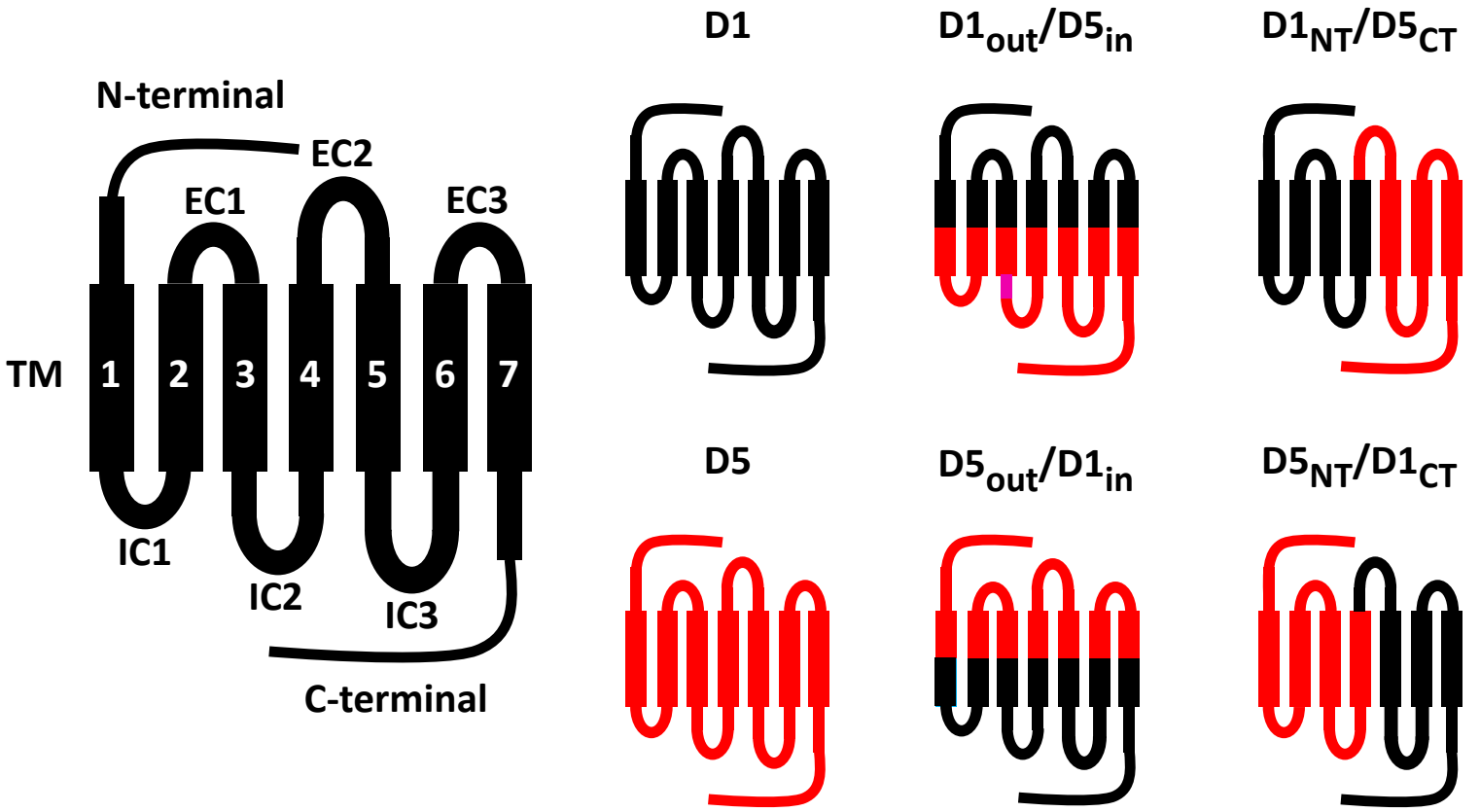
N-terminal
EC2
EC1
EC3
TM
1
2
3
4
5
6
7
IC1
IC2
IC3
C-terminal
D1
D1out/D5in
D1NT/D5CT
D5
D5out/D1in
D5NT/D1CT

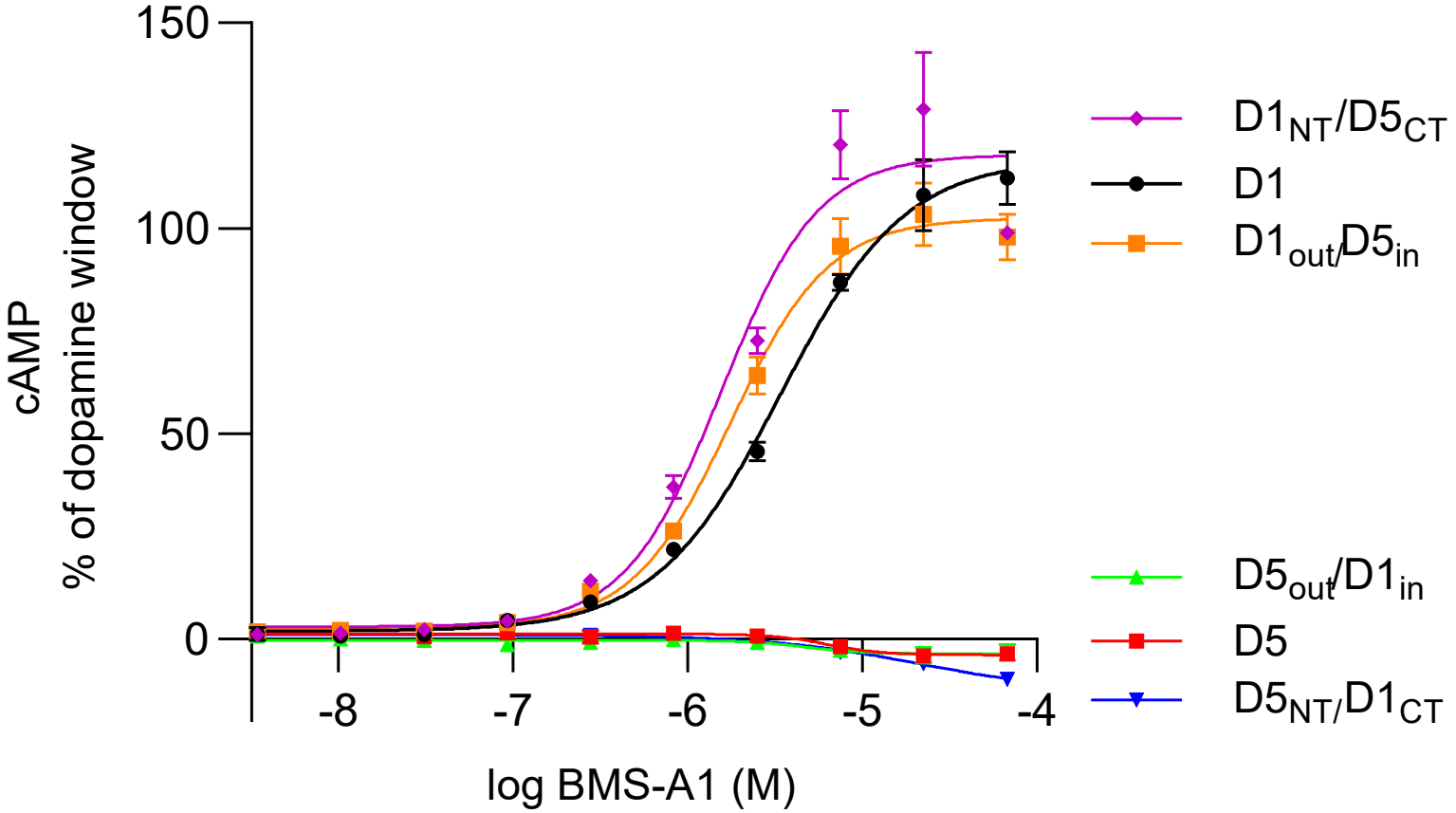
150
100
50
0
cAMP
% of dopamine window
-8
-7
-6
-5
-4
log BMS-A1 (M)
D1NT/D5CT
D1
D1out/D5in
D5out/D1in
D5
D5NT/D1CT

Figure 3

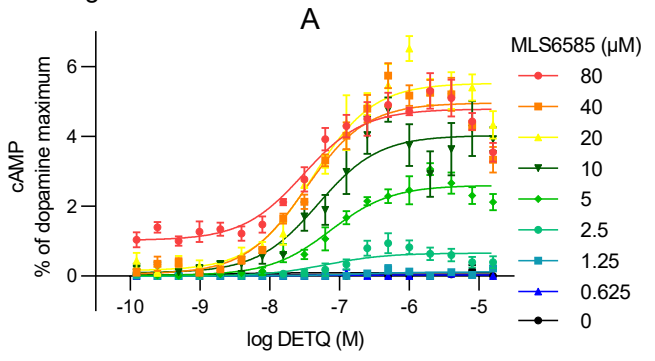
A
cAMP
% of dopamine maximum
log DETQ (M)
MLS6585 (μM)
80
40
20
10
5
2.5
1.25
0.625
0

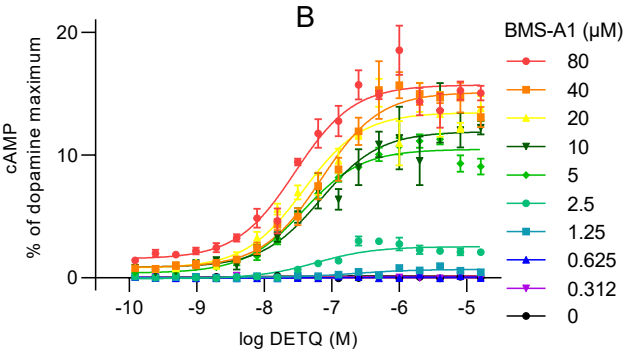
B
cAMP
% of dopamine maximum
log DETQ (M)
BMS-A1 (μM)
80
40
20
10
5
2.5
1.25
0.625
0.312
0

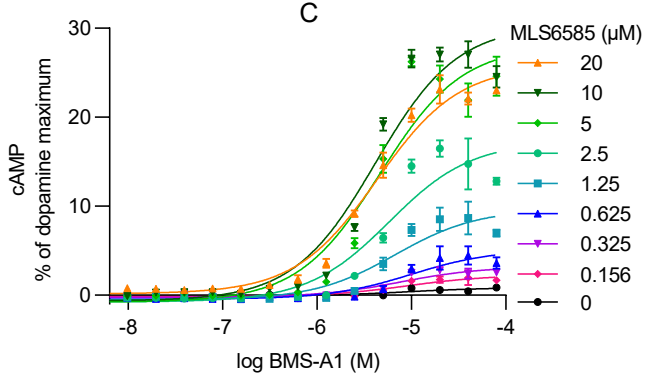
C
cAMP
% of dopamine maximum
log BMS-A1 (M)
MLS6585 (μM)
20
10
5
2.5
1.25
0.625
0.325
0.156
0

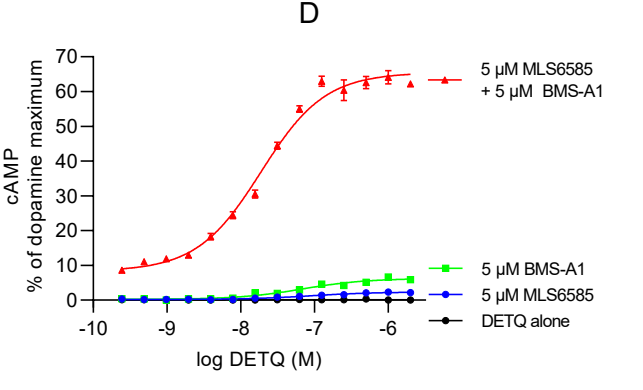
D
cAMP
% of dopamine maximum
log DETQ (M)
5 μM MLS6585
+ 5 μM BMS-A1
5 μM BMS-A1
5 μM MLS6585
DETQ alone

Figure 4

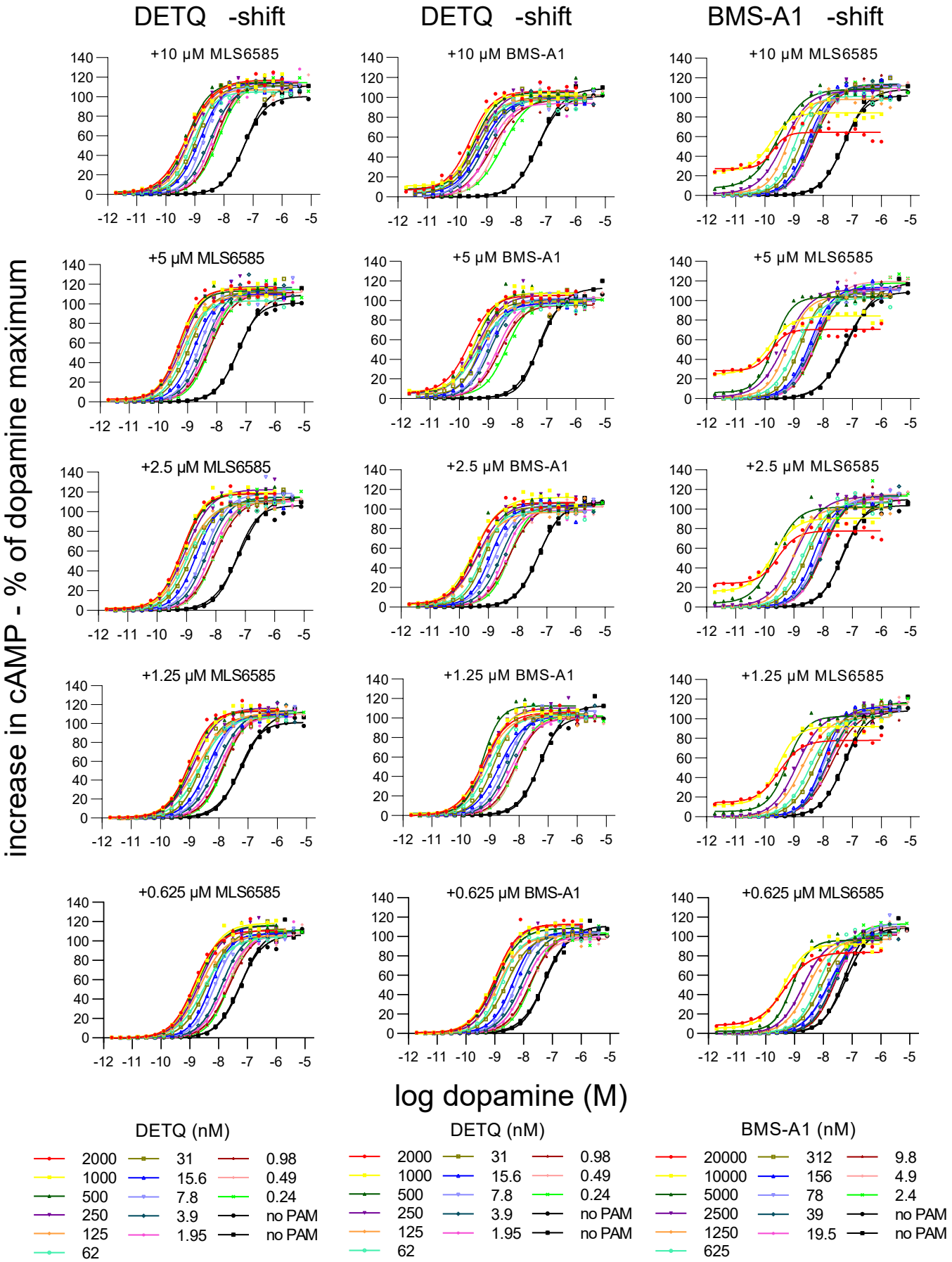
DETQ -shift
DETQ -shift
BMS-A1 -shift
+10 µM MLS6585
+10 µM BMS-A1
+10 µM MLS6585
+5 µM MLS6585
+5 µM BMS-A1
+5 µM MLS6585
+2.5 µM MLS6585
+2.5 µM BMS-A1
+2.5 µM MLS6585
+1.25 µM MLS6585
+1.25 µM BMS-A1
+1.25 µM MLS6585
+0.625 µM MLS6585
+0.625 µM BMS-A1
+0.625 µM MLS6585
increase in cAMP - % of dopamine maximum
log dopamine (M)
DETQ (nM)
2000
1000
500
250
125
62
31
15.6
7.8
3.9
1.95
0.98
0.49
0.24
no PAM
no PAM
DETQ (nM)
2000
1000
500
250
125
62
31
15.6
7.8
3.9
1.95
0.98
0.49
0.24
no PAM
no PAM
BMS-A1 (nM)
20000
10000
5000
2500
1250
625
312
156
78
39
19.5
9.8
4.9
2.4
no PAM
no PAM

Figure 5

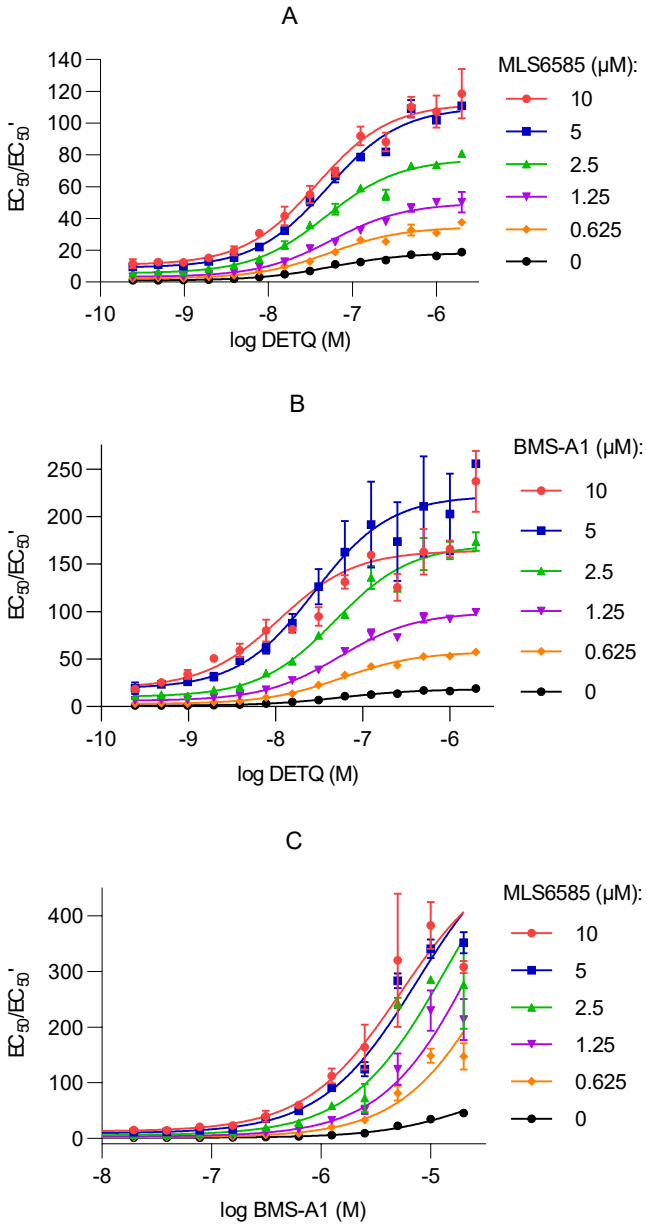
A
EC50/EC50'
log DETQ (M)
MLS6585 (μM):
10
5
2.5
1.25
0.625
0
B
EC50/EC50'
log DETQ (M)
BMS-A1 (μM):
10
5
2.5
1.25
0.625
0
C
EC50/EC50'
log BMS-A1 (M)
MLS6585 (μM):
10
5
2.5
1.25
0.625
0

Figure 6

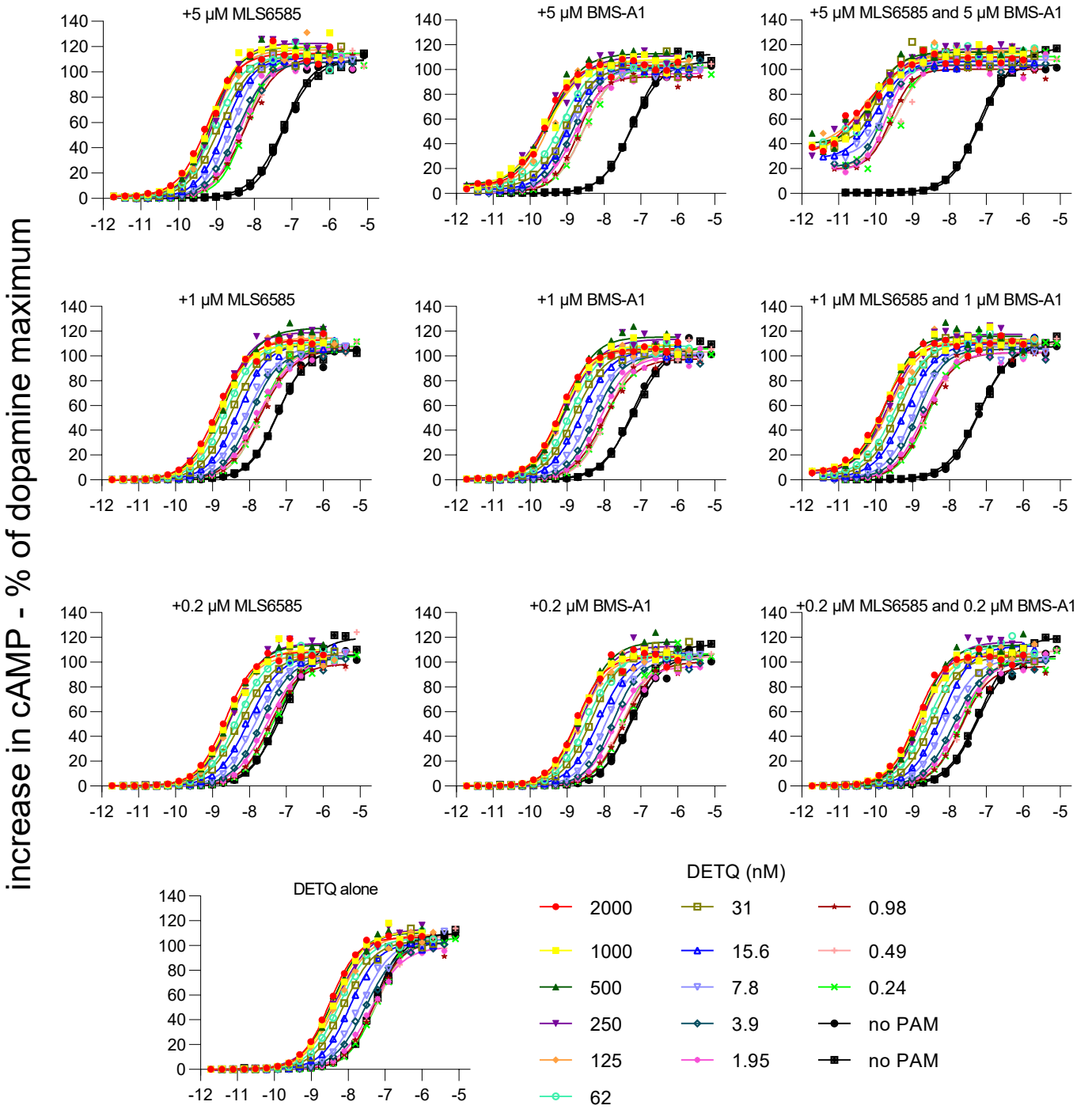
+5 µM MLS6585
+5 µM BMS-A1
+5 µM MLS6585 and 5 µM BMS-A1
+1 µM MLS6585
+1 µM BMS-A1
+1 µM MLS6585 and 1 µM BMS-A1
+0.2 µM MLS6585
+0.2 µM BMS-A1
+0.2 µM MLS6585 and 0.2 µM BMS-A1
DETQ alone
DETQ (nM)
2000
1000
500
250
125
62
31
15.6
7.8
3.9
1.95
0.98
0.49
0.24
no PAM
no PAM
increase in cAMP - % of dopamine maximum
log dopamine (M)

Figure 7

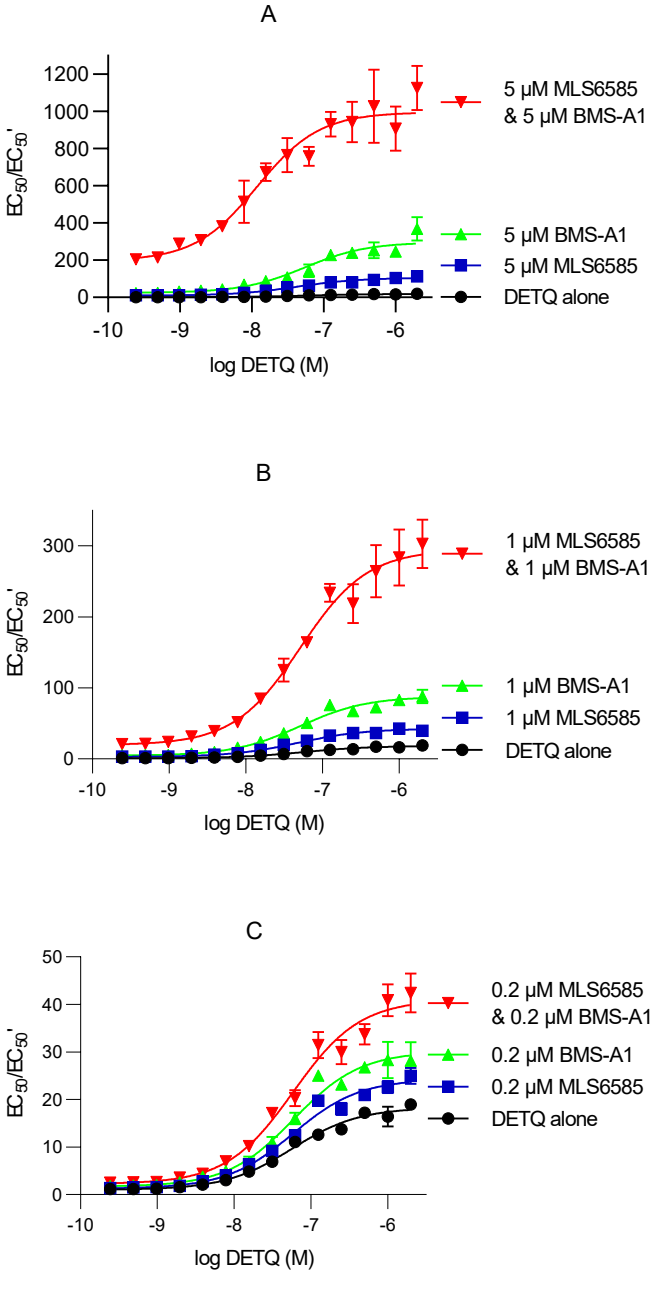
A
1200
1000
800
600
400
200
0
EC50/EC50'
-10
-9
-8
-7
-6
log DETQ (M)
5 μM MLS6585
& 5 μM BMS-A1
5 μM BMS-A1
5 μM MLS6585
DETQ alone
B
300
200
100
0
EC50/EC50'
-10
-9
-8
-7
-6
log DETQ (M)
1 μM MLS6585
& 1 μM BMS-A1
1 μM BMS-A1
1 μM MLS6585
DETQ alone
C
50
40
30
20
10
0
EC50/EC50'
-10
-9
-8
-7
-6
log DETQ (M)
0.2 μM MLS6585
& 0.2 μM BMS-A1
0.2 μM BMS-A1
0.2 μM MLS6585
DETQ alone

Molecular Pharmacology Fast Forward. Published on December 12, 2022 as DOI: 10.1124/molpharm.122.000605
This article has not been copyedited and formatted. The final version may differ from this version.

Figure 8

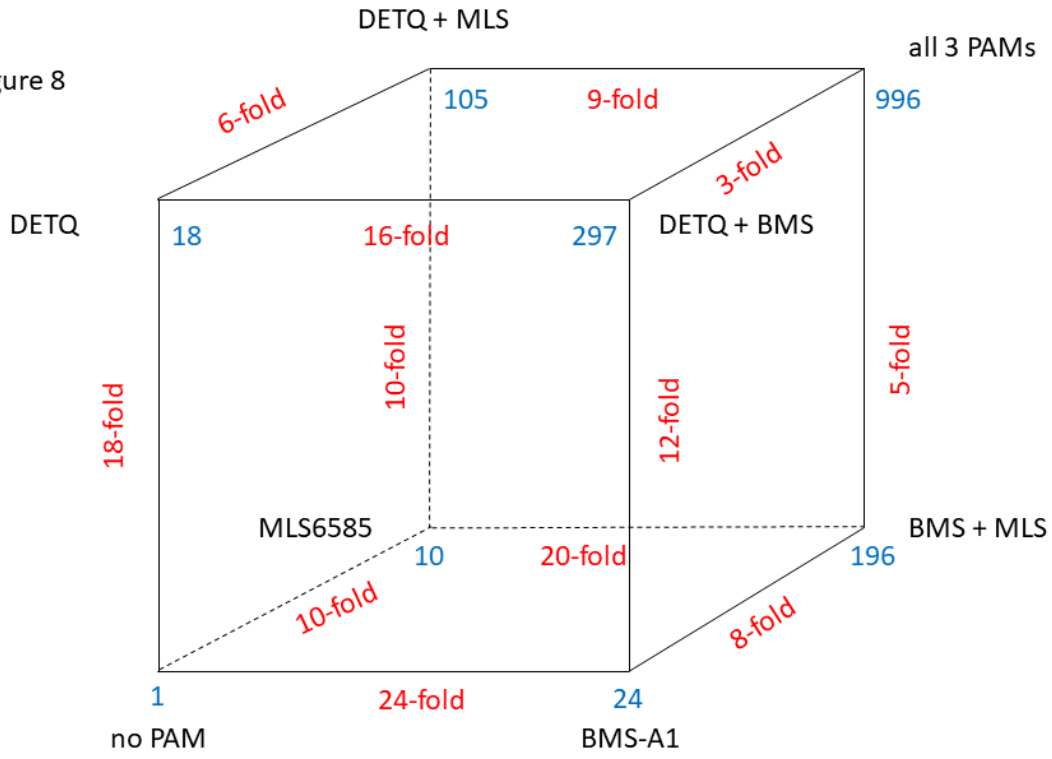

Downloaded from molpharm.aspetjournals.org at ASPET Journals on April 20, 2024

Figure 9

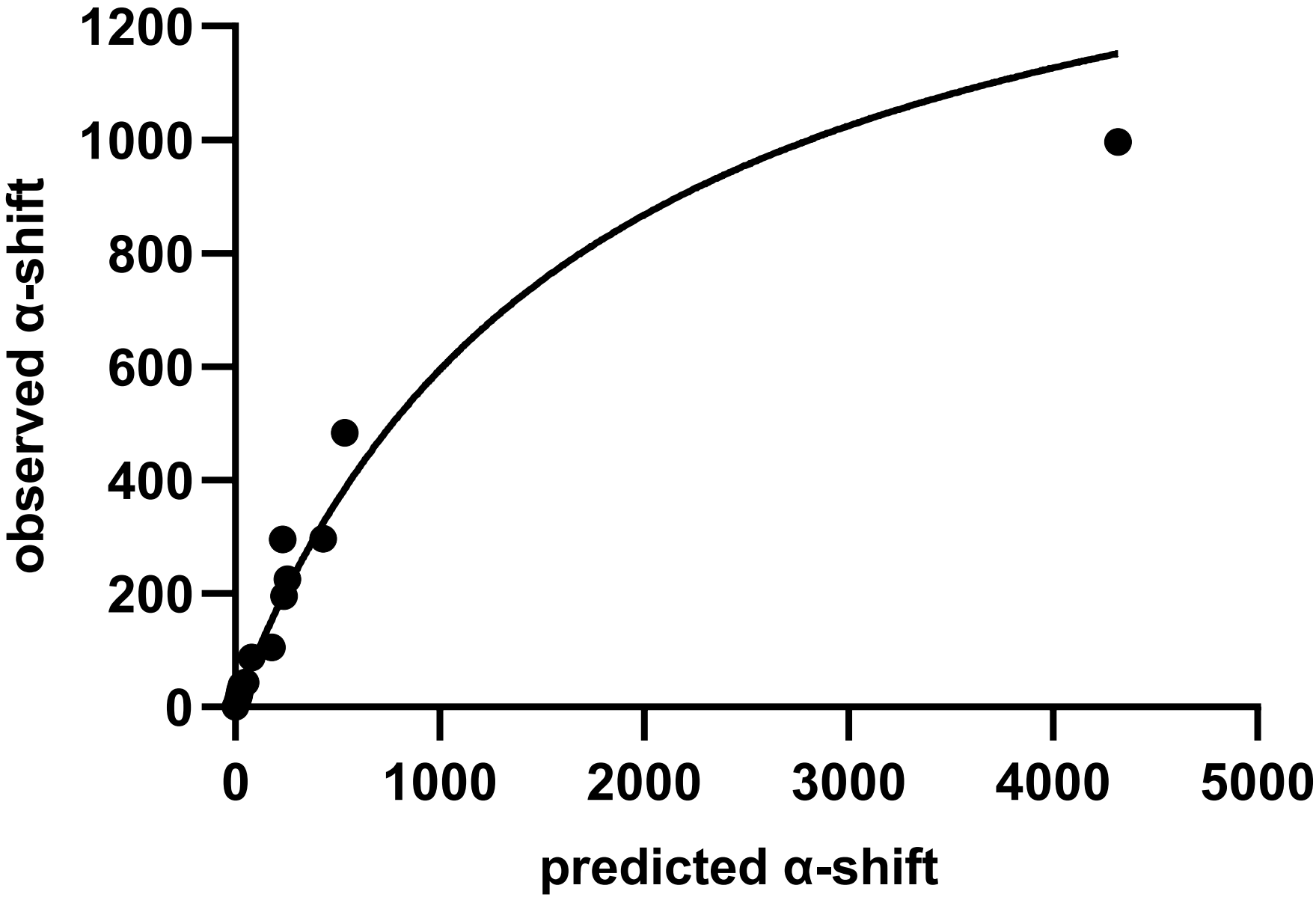
1200
1000
800
600
400
200
0
observed α-shift
0
1000
2000
3000
4000
5000
predicted α-shift

MOLPHARM-AR-2022-000605

SUPPLEMENTAL DATA

Molecular Pharmacology

Mutual Cooperativity of Three Allosteric Sites on the Dopamine D1 Receptor

Xushan Wang, Erik J Hembre, Paul J Goldsmith, James P Beck, Kjell A Svensson, Francis S Willard, Robert F Bruns

Lilly Research Laboratories, Eli Lilly & Co., Lilly Corporate Center, Indianapolis, Indiana.

Supplemental Data I: Four-Site Allosteric Model

Consider a chemical equilibrium-based model with four ligands: one orthosteric (A), and three allosteric (B, C, and D). Note the description of ligands as orthosteric/allosteric is for interpretation purposes - mathematically all four ligands are considered identical.

We assume that all four ligands bind reversibly to independent sites, and the system is at equilibrium with reciprocal cooperativity between each site.

Cooperativity between ligands is denoted by cooperativity factors (A:B α; A:C β; A:D γ; B:C δ; B:D ε; C:D θ).

This model only accounts for affinity and does not consider efficacy. Given that dopamine has efficacy ~90%, this assumption is reasonably accurate for modeling the behavior of dopamine in the presence of PAMs; however, interactions between PAMs in the absence of dopamine mostly involve increases in efficacy (see Fig. 3) and are therefore outside the domain of this model.

The system contains 20 possible components. Four free ligands (A, B, C, D), free receptor (R), four secondary species (AR, BR, CR, DR), six tertiary species (ABR, ACR, ADR, BCR, BDR, CDR), 4 quaternary species (ABCR, ABDR, ACDR, BCDR) and one quinary species (ABCDR). Derivation of the equilibrium constants for each species are conducted using standard methods (Stockton et al., 1983; Ehlert, 1988; Willard and Wainscott, 2020) incorporating the convention that cooperativity factor >1 is positive allosterism.

Each individual species can be expressed in terms of ligands, receptor, dissociation constants, and cooperativity factors:

$$[AR] = \frac{[A][R]}{K_A}$$

$$[BR] = \frac{[B][R]}{K_B}$$

$$[CR] = \frac{[C][R]}{K_C}$$

$$[DR] = \frac{[D][R]}{K_D}$$

$$[ABR] = \frac{\alpha[A][B][R]}{K_A K_B}$$

$$[ACR] = \frac{\beta[A][C][R]}{K_A K_C}$$

$$[ADR] = \frac{\gamma[A][D][R]}{K_A K_D}$$

$$[BCR] = \frac{\delta[B][C][R]}{K_B K_C}$$

$$[BDR] = \frac{\varepsilon[B][D][R]}{K_B K_D}$$

$$[CDR] = \frac{\theta[C][D][R]}{K_C K_D}$$

$$[ABCR] = \frac{\alpha\beta\delta[A][B][C][R]}{K_A K_B K_C}$$

$$[ABDR] = \frac{\alpha\gamma\varepsilon[A][B][D][R]}{K_A K_B K_D}$$

$$[ACDR] = \frac{\beta\gamma\theta[A][C][D][R]}{K_A K_C K_D}$$

$$[BCDR] = \frac{\delta\varepsilon\theta[B][C][D][R]}{K_B K_C K_D}$$

$$[ABCDR] = \frac{\alpha\beta\gamma\delta\varepsilon\theta[A][B][C][D][R]}{K_A K_B K_C K_D}$$

For simplification, we assume that only A-containing species account for activated receptors:

$$Fraction\ of\ receptors\ occupied\ (\rho) = \frac{\sum AR\ species}{R_T}$$

$$\rho = \frac{[AR] + [ABR] + [ACR] + [ADR] + [ABCR] + [ABDR] + [ACDR] + [ABDCR]}{[R] + [AR] + [BR] + [CR] + [DR] + [ABR] + [ACR] + [ADR] + [BCR] + [BDR] + [CDR] + [ABCR] + [ABDR] + [ACDR] + [BCDR] + [ABCDR]}$$

Equation 1

$$\rho = \frac{\frac{[A]}{K_A} + \frac{\alpha[A][B]}{K_AK_B} + \frac{\beta[A][C]}{K_AK_C} + \frac{\gamma[A][D]}{K_AK_D} + \frac{\alpha\beta\delta[A][B][C]}{K_AK_BK_C} + \frac{\alpha\gamma\varepsilon[A][B][D]}{K_AK_BK_D} + \frac{\beta\gamma\theta[A][C][D]}{K_AK_CK_D} + \frac{\alpha\beta\gamma\delta\varepsilon\theta[A][B][C][D]}{K_AK_BK_CK_D}}{1 + \frac{[A]}{K_A} + \frac{[B]}{K_B} + \frac{[C]}{K_C} + \frac{[D]}{K_D} + \frac{\alpha[A][B]}{K_AK_B} + \frac{\beta[A][C]}{K_AK_C} + \frac{\gamma[A][D]}{K_AK_D} + \frac{\delta[B][C]}{K_BK_C} + \frac{\varepsilon[B][D]}{K_BK_D} + \frac{\theta[C][D]}{K_CK_D} + \frac{\alpha\beta\delta[A][B][C]}{K_AK_BK_C} + \frac{\alpha\gamma\varepsilon[A][B][D]}{K_AK_BK_D} + \frac{\beta\gamma\theta[A][C][D]}{K_AK_CK_D} + \frac{\delta\varepsilon\theta[B][C][D]}{K_BK_CK_D} + \frac{\alpha\beta\gamma\delta\varepsilon\theta[A][B][C][D]}{K_AK_BK_CK_D}}$$

For each ligand, the half maximal concentration for receptor occupancy is denoted by the X_{50}.

For A, this is defined by the 8 A-containing species (*vide supra*) and for B, C, and D, the 4 AB, AC, AD containing species respectively, consistent with the model assumptions (*vide supra*).

Equation 2

$$A_{50} = K_A\left(\frac{1 + \frac{[B]}{K_B} + \frac{[C]}{K_C} + \frac{[D]}{K_D} + \frac{\delta[B][C]}{K_BK_C} + \frac{\varepsilon[B][D]}{K_BK_D} + \frac{\theta[C][D]}{K_CK_D} + \frac{\delta\varepsilon\theta[B][C][D]}{K_BK_CK_D}}{1 + \frac{\alpha[B]}{K_B} + \frac{\beta[C]}{K_C} + \frac{\gamma[D]}{K_D} + \frac{\alpha\beta\delta[B][C]}{K_BK_C} + \frac{\alpha\gamma\varepsilon[B][D]}{K_BK_D} + \frac{\beta\gamma\theta[C][D]}{K_CK_D} + \frac{\alpha\beta\gamma\delta\varepsilon\theta[B][C][D]}{K_BK_CK_D}}\right)$$

Equation 3

$$B_{50} = K_B\left(\frac{1 + \frac{[A]}{K_A} + \frac{[C]}{K_C} + \frac{[D]}{K_D} + \frac{\beta[A][C]}{K_AK_C} + \frac{\gamma[A][D]}{K_AK_D} + \frac{\theta[C][D]}{K_CK_D} + \frac{\beta\gamma\theta[A][C][D]}{K_AK_CK_D}}{-1 - \frac{\alpha[A]}{K_A} - \frac{\delta[C]}{K_C} - \frac{\varepsilon[D]}{K_D} + \frac{\alpha\beta\delta[A][C]}{K_AK_C} + \frac{\alpha\gamma\varepsilon[A][D]}{K_AK_D} - \frac{\delta\varepsilon\theta[C][D]}{K_CK_D} + \frac{\alpha\beta\gamma\delta\varepsilon\theta[A][C][D]}{K_AK_CK_D}}\right)$$

Other applications of the model are possible, ***e.g.*** including all liganded receptor species contributing to receptor activation:

Equation 4

$$\rho = \frac{\frac{[A]}{K_A} + \frac{[B]}{K_B} + \frac{[C]}{K_C} + \frac{[D]}{K_D} + \frac{\alpha[A][B]}{K_AK_B} + \frac{\beta[A][C]}{K_AK_C} + \frac{\gamma[A][D]}{K_AK_D} + \frac{\delta[B][C]}{K_BK_C} + \frac{\varepsilon[B][D]}{K_BK_D} + \frac{\theta[C][D]}{K_CK_D} + \frac{\alpha\beta\delta[A][B][C]}{K_AK_BK_C} + \frac{\alpha\gamma\varepsilon[A][B][D]}{K_AK_BK_D} + \frac{\beta\gamma\theta[A][C][D]}{K_AK_CK_D} + \frac{\delta\varepsilon\theta[B][C][D]}{K_BK_CK_D} + \frac{\alpha\beta\gamma\delta\varepsilon\theta[A][B][C][D]}{K_AK_BK_CK_D}}{1 + \frac{[A]}{K_A} + \frac{[B]}{K_B} + \frac{[C]}{K_C} + \frac{[D]}{K_D} + \frac{\alpha[A][B]}{K_AK_B} + \frac{\beta[A][C]}{K_AK_C} + \frac{\gamma[A][D]}{K_AK_D} + \frac{\delta[B][C]}{K_BK_C} + \frac{\varepsilon[B][D]}{K_BK_D} + \frac{\theta[C][D]}{K_CK_D} + \frac{\alpha\beta\delta[A][B][C]}{K_AK_BK_C} + \frac{\alpha\gamma\varepsilon[A][B][D]}{K_AK_BK_D} + \frac{\beta\gamma\theta[A][C][D]}{K_AK_CK_D} + \frac{\delta\varepsilon\theta[B][C][D]}{K_BK_CK_D} + \frac{\alpha\beta\gamma\delta\varepsilon\theta[A][B][C][D]}{K_AK_BK_CK_D}}$$

Examples:

Using Equation 2 for AC_{50} we can model the interactions of the 4 ligands under conditions approximated from the D1R, dopamine, DETQ, BMS, MLS example:

K_A (50 nM), K_B (100 nM), K_C (7 μM), K_D (2.5 μM), α (18), β (30), γ (11), δ (18), ε (6), θ (7).

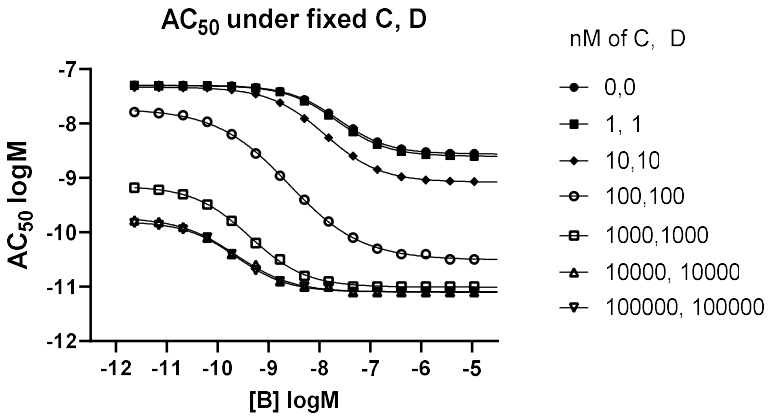

	0,0	1, 1	10,10	100,100	1000,1000	10000, 10000	100000, 100000
Bottom	-8.561	-8.604	-9.078	-10.51	-11.01	-11.10	-11.10
Top	-7.298	-7.303	-7.332	-7.728	-9.149	-9.730	-9.803
LogEC50	-7.624	-7.654	-7.890	-8.599	-9.371	-9.646	-9.636
HillSlope	-0.8787	-0.8725	-0.7966	-0.6080	-0.7892	-0.7772	-0.8564
EC50	2.378e-008	2.218e-008	1.288e-008	2.518e-009	4.259e-010	2.258e-010	2.312e-010

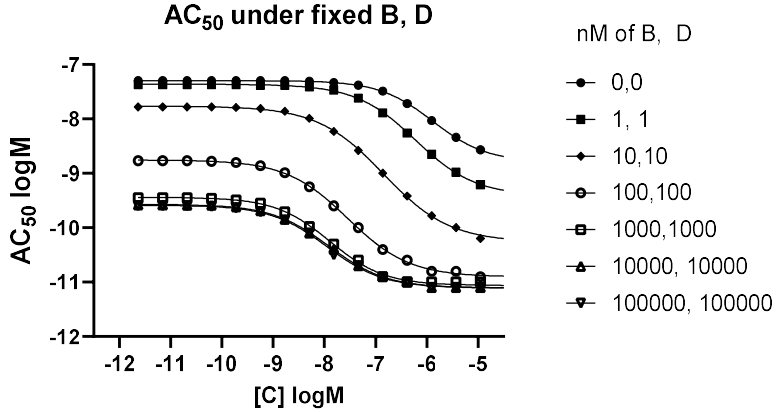

	0,0	1, 1	10,10	100,100	1000,1000	10000, 10000	100000, 100000
Bottom	-8.791	-9.414	-10.26	-10.91	-11.06	-11.11	-11.10
Top	-7.297	-7.363	-7.765	-8.755	-9.443	-9.571	-9.587
LogEC50	-5.883	-6.223	-6.845	-7.545	-7.892	-7.911	-7.954
HillSlope	-0.8271	-0.7432	-0.6731	-0.7207	-0.8124	-0.7720	-0.7881
EC50	1.309e-006	5.986e-007	1.429e-007	2.852e-008	1.282e-008	1.228e-008	1.111e-008

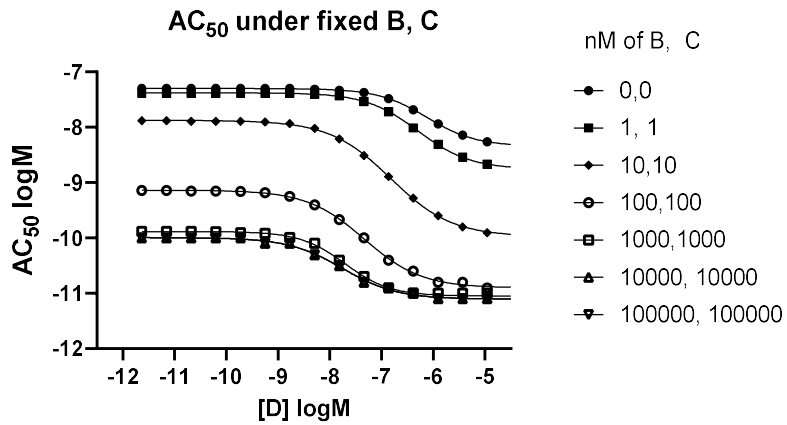

	0,0	1, 1	10,10	100,100	1000,1000	10000, 10000	100000, 100000
Bottom	-8.341	-8.756	-9.974	-10.90	-11.05	-11.10	-11.10
Top	-7.299	-7.376	-7.875	-9.137	-9.883	-9.995	-9.995
LogEC50	-6.124	-6.294	-6.822	-7.334	-7.705	-7.754	-7.754
HillSlope	-0.9161	-0.8569	-0.7339	-0.7820	-0.9940	-0.8236	-0.8236
EC50	7.513e-007	5.080e-007	1.505e-007	4.634e-008	1.972e-008	1.760e-008	1.760e-008

We can observe the allosteric synergy and saturability of the response in all combinations of ligands. In the absence of effective B, C, D the AC_{50} is K_A (in this case 50 nM, -7.3 log M). Similarly, plateau values for single combinations of A with B, C, or D are observed (-8.6, -8.8, and -8.3 respectively). A maximal asymptote of 8 pM (-11.1 log M) is observed at saturating concentrations of the four ligands.

We can also use an occupancy model (Equation1) to simulate experiments. Simulation of several experimental conditions gave output qualitatively similar to experimental data.

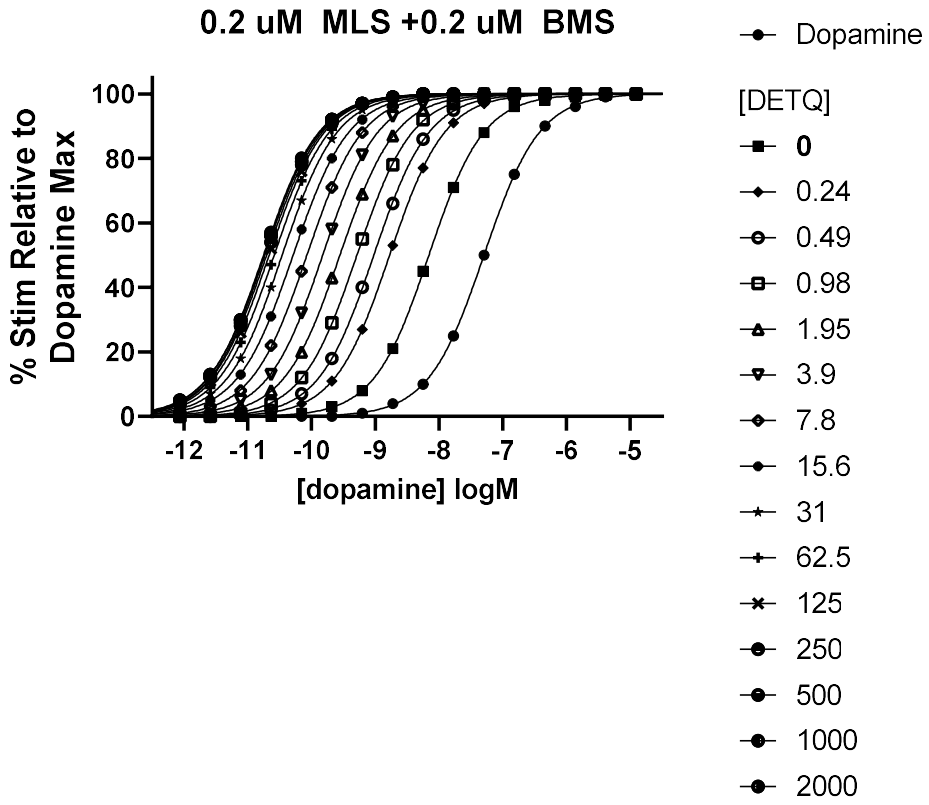

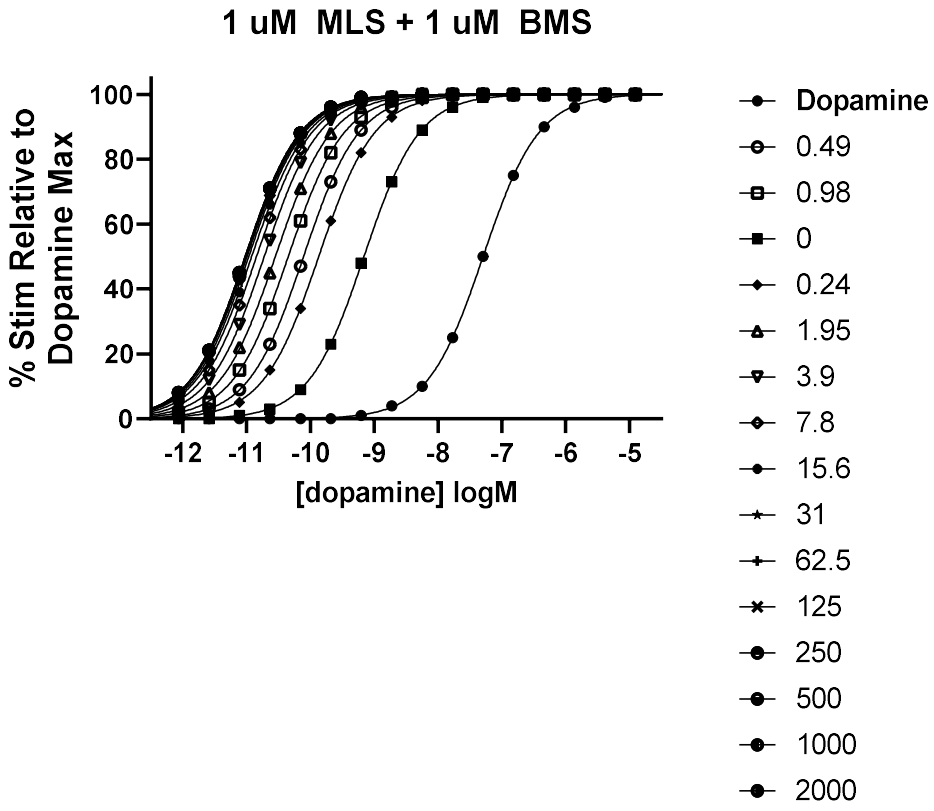

We note that 50 pM (essentially 1000-fold affinity enhancement) was the highest potency value for dopamine determined experimentally whereas 8 pM was calculated as maximum potency from the model. The model we use has many assumptions including equilibrium, a random order of binding, and reciprocal multiplicative cooperativity.

Overall this model provides an initial theoretical construct for further analysis of the pharmacology.

Ehlert FJ (1988) Estimation of the affinities of allosteric ligands using radioligand binding and pharmacological null methods. *Mol Pharmacol* **33**:187-194.

Stockton JM, Birdsall NJ, Burgen AS and Hulme EC (1983) Modification of the binding properties of muscarinic receptors by gallamine. *Mol Pharmacol* **23**:551-557.

Willard FS and Wainscott DB (2020) G protein-coupled receptor allosteric modulators: understanding modulator affinity and pharmacological dose, in *GPCRs* pp 271-282, Elsevier.

Supplemental Data II: Synthesis of BMS-A1 and Stereoisomers

Reaction scheme:

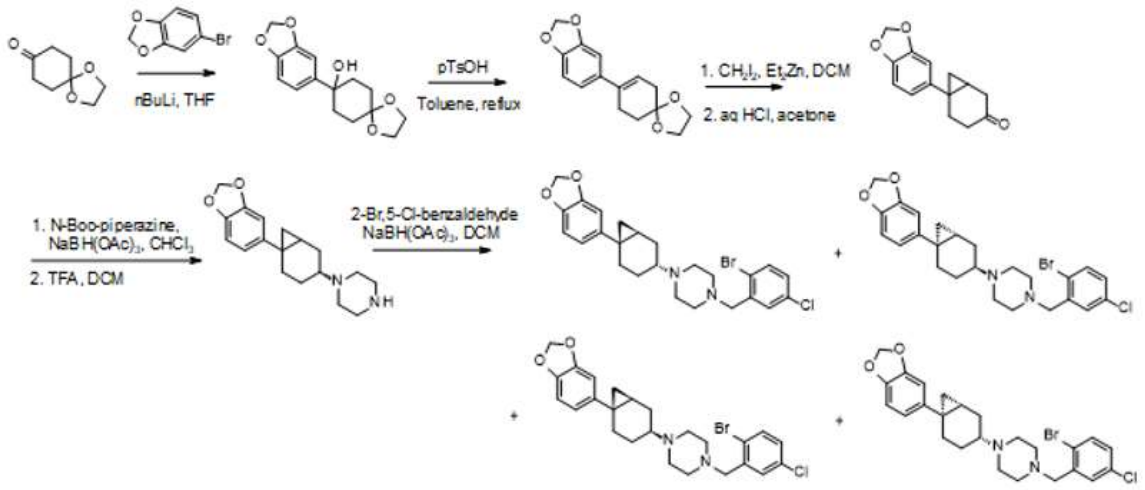

Step 1 (Aryl lithium addition)**: 8-(1,3-benzodioxol-5-yl)-1,4-dioxaspiro[4.5]decan-8-ol**

To a stirred solution of 4-bromo-1,2-(methylenedioxy)benzene (4.99 g, 24.8 mmol) in anhydrous THF (60 mL) at -78 °C under an atmosphere of N_2, was added n-butyllithium (20 mL of a 2.5M soln. in hexanes, 49.6 mmol, 2.5 mol/L) over 5 minutes. The resulting opaque yellow mixture was stirred at -78 °C for 1 h and then 1,4-dioxaspiro[4.5]decan-8-one (3.88 g, 24.8 mmol) was added in a dropwise fashion as a solution in anhydrous THF (10 mL) over 5 minutes. The reaction mixture was stirred at -78 °C for 2 h, then the cooling bath was removed, and the reaction mixture was stirred while warming to RT. After 1 h, an aliquot was removed and MS analysis showed the reaction was complete. The reaction mixture was quenched with aqueous 20% NH_4Cl (50 mL) and brine (50 mL), and the mixture was extracted with EtOAc (100 mL). The organic layer was dried over Na_2SO_4, filtered, and concentrated. The resulting residue was purified by silica column (120 g, 50-100% EtOAc in hexanes) to provide 8-(1,3-benzodioxol-

5-yl)-1,4-dioxaspiro[4.5]decan-8-ol (6.19 g, 20.00 mmol, 81% yield) as a pale yellow oil.

MS: Obs m/z 301 $[M+Na]^+$

1H NMR (400 MHz; $CDCl_3$): consistent with product plus minor impurity. Product denoted as 90% purity.

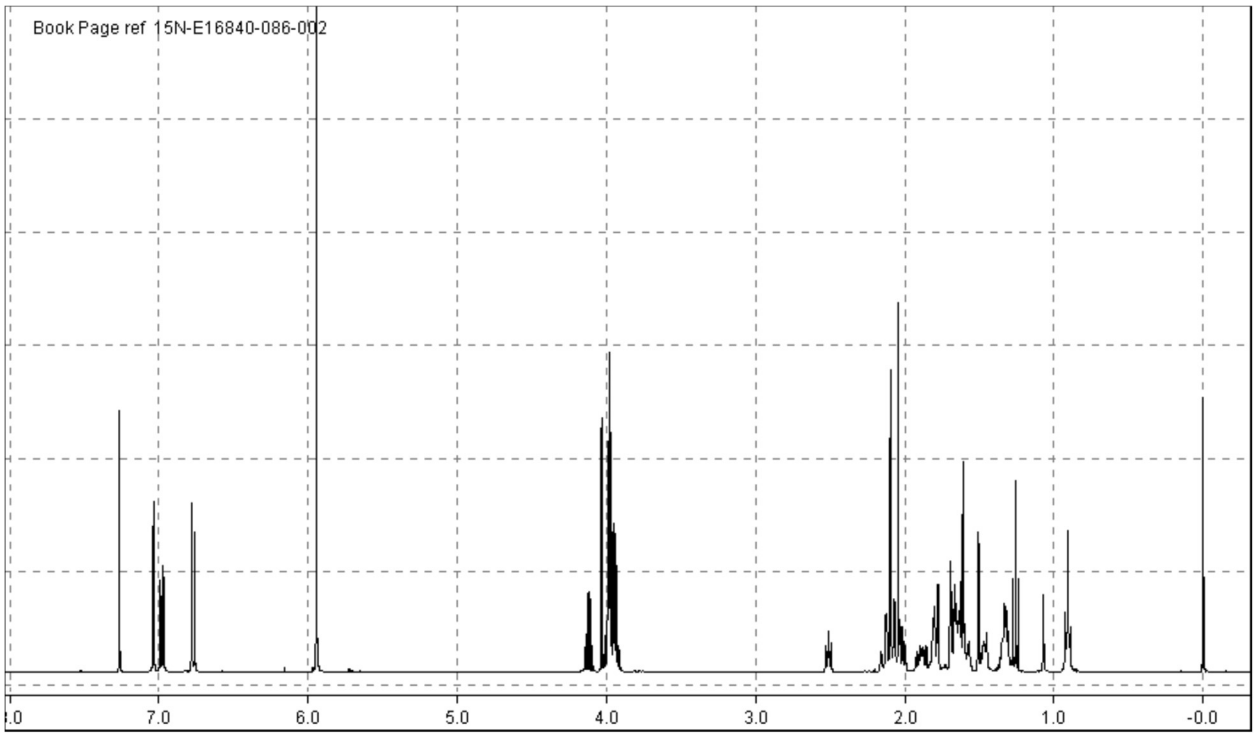

Step 2 (Dehydration): **8-(1,3-benzodioxol-5-yl)-1,4-dioxaspiro[4.5]dec-7-ene**

To a stirred solution of 8-(1,3-benzodioxol-5-yl)-1,4-dioxaspiro[4.5]decan-8-ol (2.39 g, 7.71 mmol) in toluene (60 mL) was added p-toluenesulfonic acid (0.134 g, 0.771 mmol). The reaction mixture was heated to reflux and stirred for 2.5 h, at which time analysis of an aliquot by MS showed complete consumption of starting material. The reaction mixture was cooled to room temp. and concentrated to provide a purple residue that was purified by silica column (120 g, 0-50% EtOAc in hexanes) to provide 8-(1,3-benzodioxol-5-yl)-1,4-dioxaspiro[4.5]dec-7-ene (1.61 g, 6.18 mmol, 80.09% Yield) as a yellow oil.

MS: Obs m/z 261 $[M+H]^+$

1H NMR (400 MHz; $CDCl_3$): consistent with product

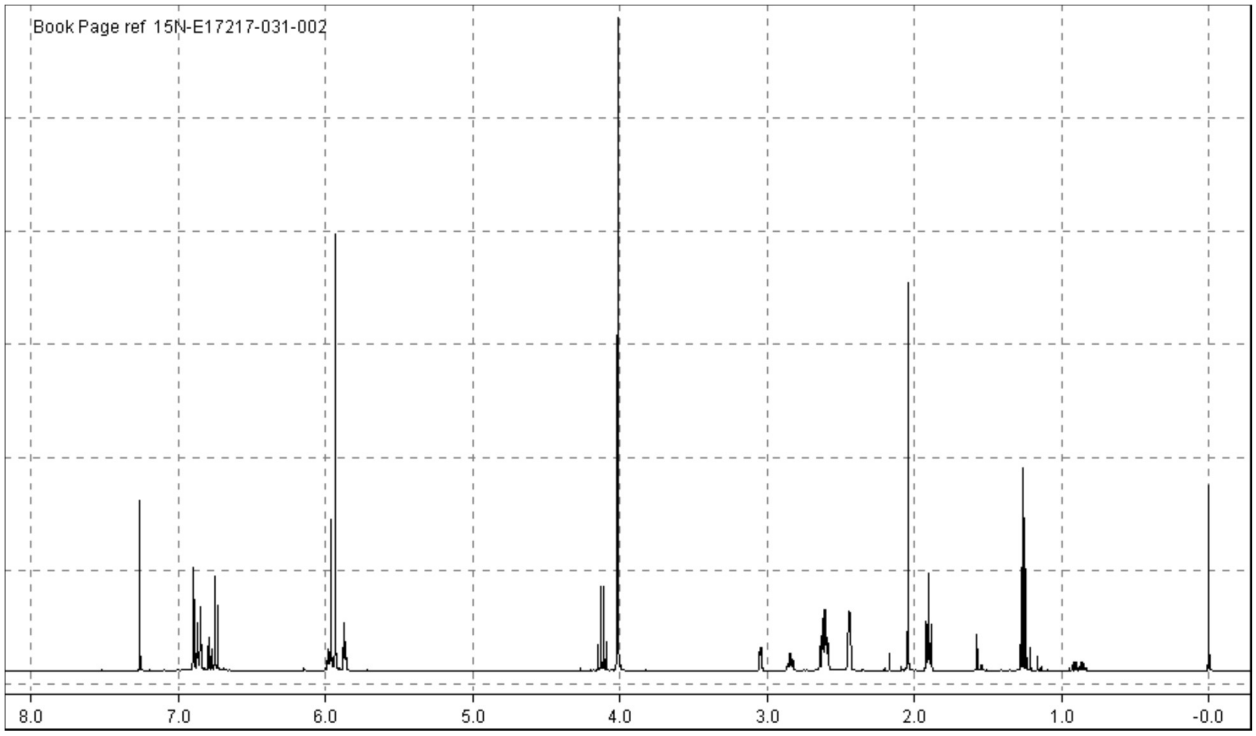

Steps 3 and 4 (Simmons-Smith cyclopropanation and acetal cleavage): **6-(1,3-benzodioxol-5-yl)norcaran-3-one**

To a stirred solution of diethylzinc (19.4 mL of a 15 wt.% soln in toluene, 21.6 mmol) in anhydrous dichloromethane (20 mL) at 0 °C under N_2, a solution of trifluoroacetic acid (2.45 g, 1.63 mL, 21.5 mmol) in dichloromethane (10 mL) was carefully added in a dropwise fashion. The mixture was stirred at 0 °C for 20 min. and then a solution of diiodomethane (5.76 g, 1.73 mL, 21.5 mmol) in dichloromethane (10 mL) was added. After stirring for another 20 min., a solution of 8-(1,3-benzodioxol-5-yl)-1,4-dioxaspiro[4.5]dec-7-ene (2.80 g, 10.8 mmol) in dichloromethane (10 mL) was added. The cooling bath was removed, and the reaction mixture was stirred at RT for 2.5 h. The reaction mixture was carefully quenched with saturated aqueous $NaHCO_3$ (100 mL) and water (50 mL). The biphasic heterogeneous mixture was vigorously stirred overnight. The resulting mixture was filtered to remove undissolved solid, and the organic layer in the filtrate was separated using a hydrophobic frit and concentrated. The resulting residue was purified by silica column (120 g; 0-40% EtOAc in hexanes) to provide 2.95 g of a mixture of acetal and ketone as a colorless oil. The mixture was dissolved in acetone (50 mL) and 2M aqueous hydrochloric acid (20 mL, 40 mmol) was added. The mixture was stirred at RT for 1 h and then

concentrated to remove the acetone. The residue was diluted with brine (50 mL) and extracted with dichloromethane (50 mL). The organic layer was separated, dried, and concentrated to provide 6-(1,3-benzodioxol-5-yl)norcaran-3-one (1.824 g, 7.920 mmol, 73.6% yield) as a yellow solid that was advanced to the next step without further purification.

MS: (ketone product) Obs m/z 231 $[M+H]^+$

1H NMR (400 MHz; $CDCl_3$): consistent with product plus minor impurities.

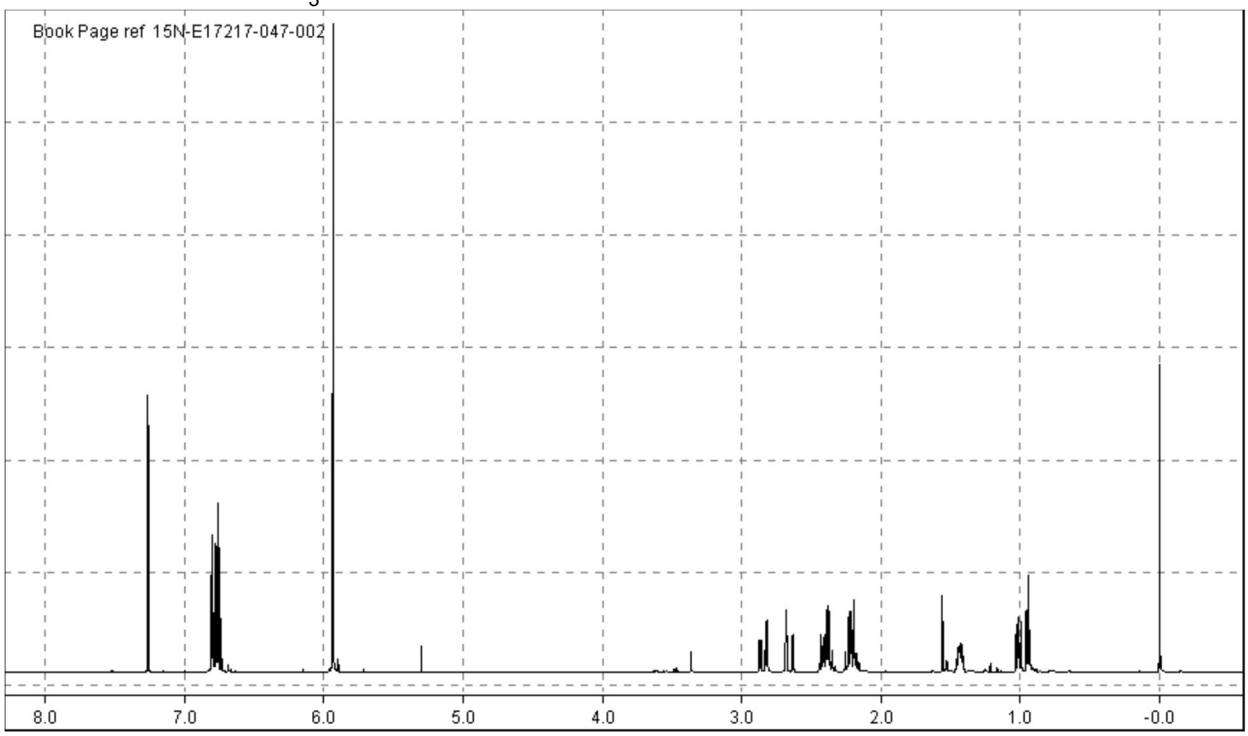

Step 5 (reductive amination): tert-butyl 4-[6-(1,3-benzodioxol-5-yl)norcaran-3-yl]piperazine-1-carboxylate To a stirred solution of 6-(1,3-benzodioxol-5-yl)norcaran-3-one (1.82 g, 7.92 mmol) and 1-Boc-piperazine (4.43 g, 23.8 mmol) in chloroform (60 mL) at RT, was added sodium triacetoxyborohydride (5.036 g, 23.76 mmol). The reaction mixture was heated at reflux temperature overnight (18 h) and then cooled to RT and quenched with saturated aqueous $NaHCO_3$ (100 mL). The organic layer was separated (hydrophobic frit) and concentrated. The resulting residue was purified by silica column (120 g; 50-100% EtOAc in hexanes) to provide tert-butyl 4-[6-(1,3-benzodioxol-5-yl)norcaran-3-yl]piperazine-1-carboxylate (2.81 g, 7.02 mmol, 88.7% yield) as a mixture of syn- and anti-diastereomers as a yellow gum.

MS: Obs m/z 401 $[M+H]^+$

1H NMR (400 MHz; $CDCl_3$): consistent with product as a mixture of diastereoisomers plus some residual EtOAc.

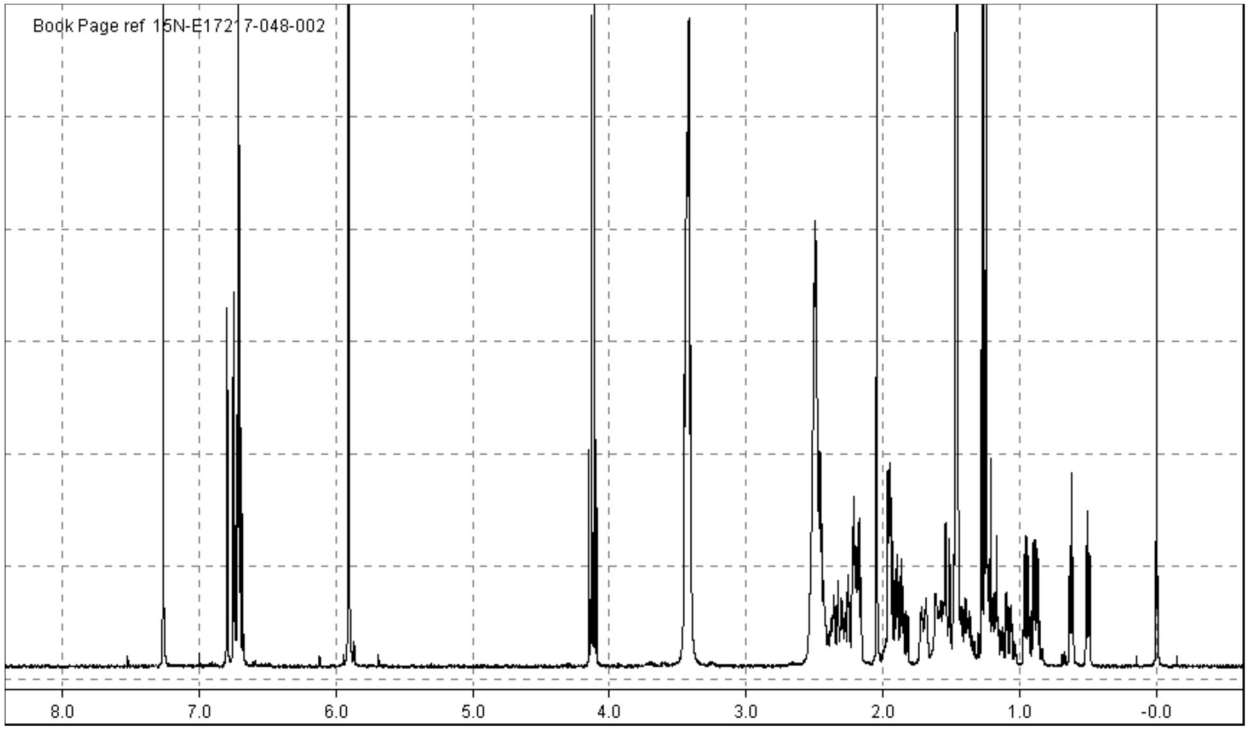

Step 6 (Boc deprotection): 1-[6-(1,3-benzodioxol-5-yl)norcaran-3-yl]piperazine

To a stirred solution of tert-butyl 4-[6-(1,3-benzodioxol-5-yl)norcaran-3-yl]piperazine-1-carboxylate (2.932 g, 7.321 mmol) in dichloromethane (20 mL) at RT was added trifluoroacetic acid (7.54 g, 5 mL, 66.1 mmol). The reaction mixture was stirred at RT over the weekend (66 h). Analysis of an aliquot by MS (low pH) showed that all SM was consumed. The reaction mixture was concentrated, and the resulting residue was purified by SCX-2 column (50 g; loaded/washed with MeOH; eluted with 2M NH_3 in MeOH then concentrated) to provide 1-[6-(1,3-benzodioxol-5-yl)norcaran-3-yl]piperazine (2.07 g, 6.90 mmol, 94.3% yield) as a mixture of syn- and anti-diastereomers as a thick orange oil.

MS: Obs m/z 301 $[M+H]^+$

1H NMR (400 MHz; $CDCl_3$): consistent with product (approx 1:1 mixture of diastereomers).

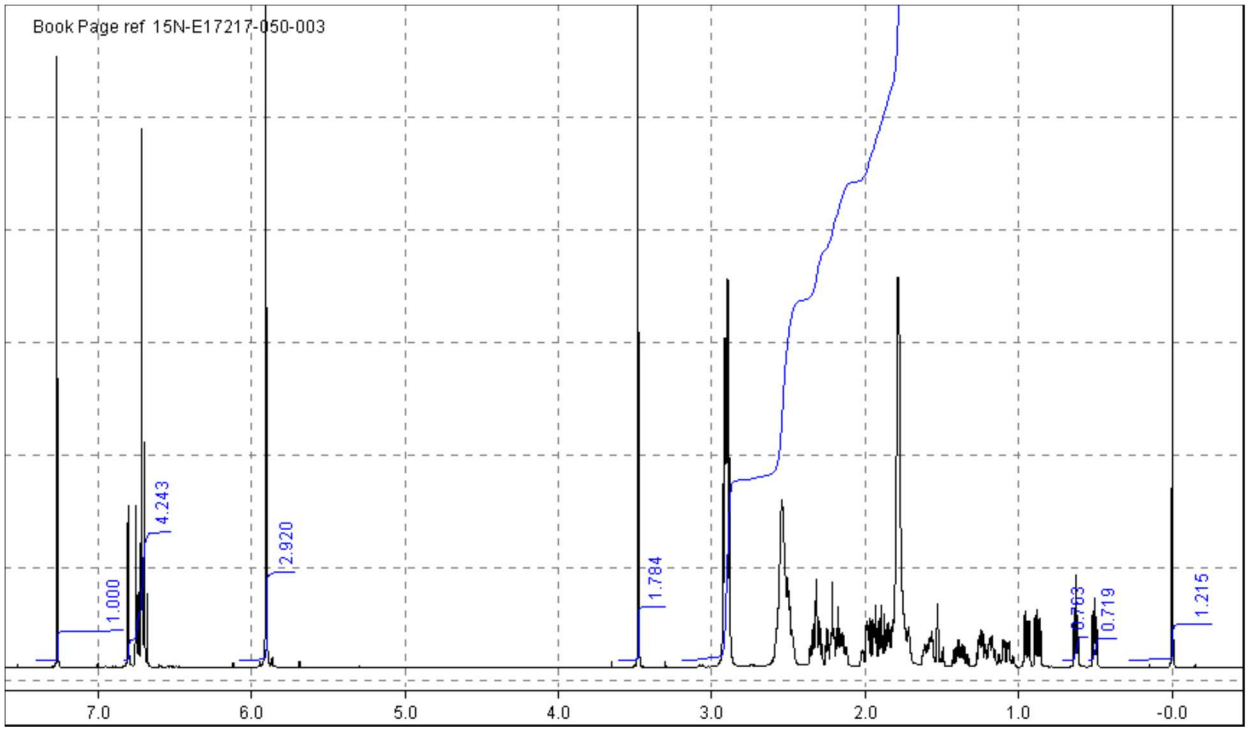

Step 7 (reductive amination): 1-[6-(1,3-benzodioxol-5-yl)norcaran-3-yl]-4-[(2-bromo-5-chloro-phenyl)methyl]piperazine (four isomers)

To a stirred solution of 1-[6-(1,3-benzodioxol-5-yl)norcaran-3-yl]piperazine (2.07 g, 6.90) in dichloromethane (60 mL) at RT, was added sodium triacetoxyborohydride (2.048 g, 9.663 mmol) and 2-bromo-5-chlorobenzaldehyde (2.14 g, 9.66 mmol). The reaction mixture was stirred at RT overnight (18 h) and then quenched with MeOH (30 mL) and purified directly by SCX-2 column (50 g; loaded/washed with MeOH; eluted with 2M NH_3 in MeOH then concentrated). The resulting residue was purified by silica column (120 g; 50-100% EtOAc in hexanes) to provide 1-[6-(1,3-benzodioxol-5-yl)norcaran-3-yl]-4-[(2-bromo-5-chloro-phenyl)methyl]piperazine (2.90 g, 5.75 mmol, 83.3% yield) as a mixture of syn- and anti-diastereomers as a colorless oil. This mixture was further purified by chiral HPLC [Chiralpak AD-H column (Daicel Corporation, 30 x 250 mm, 5 micron); mobile phase: 25% IPA with 0.2% DMEA; Outlet pressure: 100 bar; column temp.: 35 C; Flow rate: 125 mL/min; detection: 220 nm; loading: 75 mg injection every 4.2 min] to provide four isomers.

MS: Obs m/z 505.0 $[M+H]^+$

The isomers are named “Isomers 1-4” based on their elution order off the chiral column.

ISOMER 1

1-[6-(1,3-benzodioxol-5-yl)norcaran-3-yl]-4-[(2-bromo-5-chloro-phenyl)methyl]piperazine - Isomer 1: (0.486 g, 0.964 mmol, 14.0% yield). 2D NMR analysis shows relative stereochemistry between cyclopropyl and piperidine as *anti*.

1H NMR spectra

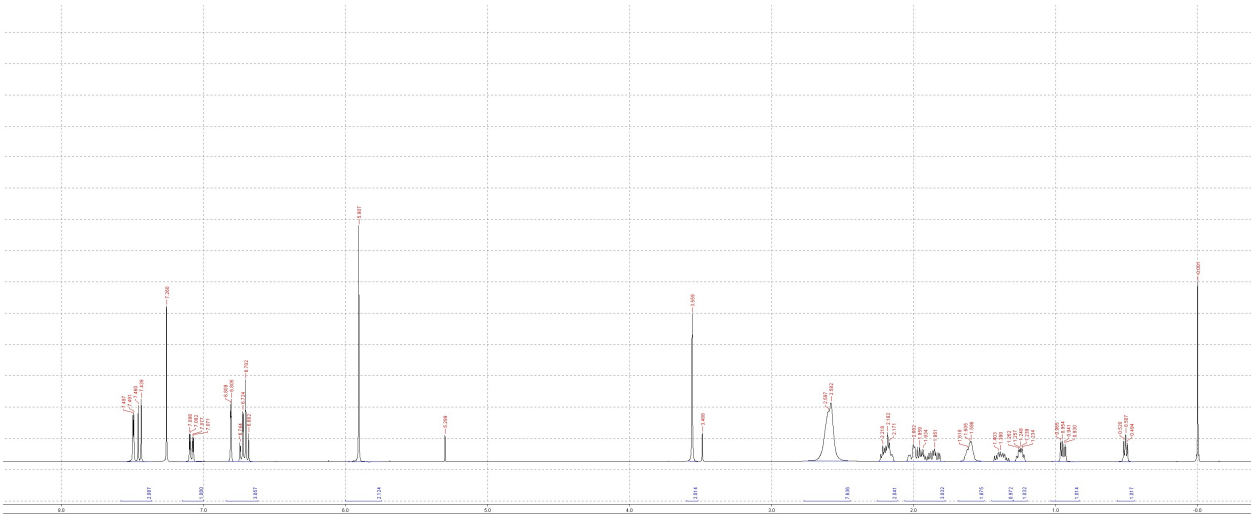

COSY spectra:

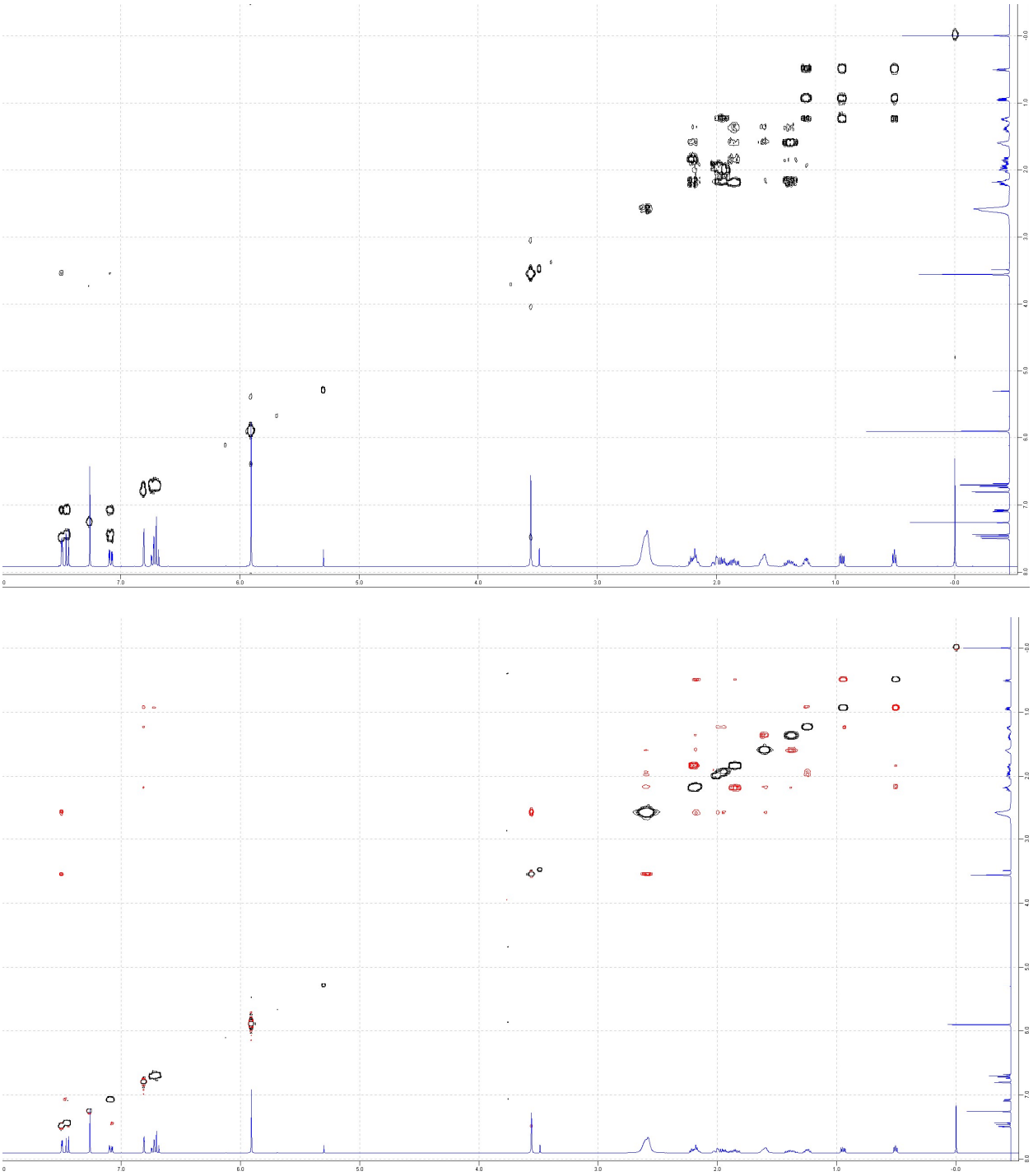

ISOMER 2: "BMS-A1"

1-[6-(1,3-benzodioxol-5-yl)norcaran-3-yl]-4-[(2-bromo-5-chloro-phenyl)methyl]piperazine - Isomer 2:

(0.489 g, 0.970 mmol, 14.1% yield). 2D NMR analysis shows relative stereochemistry between

cyclopropyl and piperidine as *anti*.

1H NMR spectra:

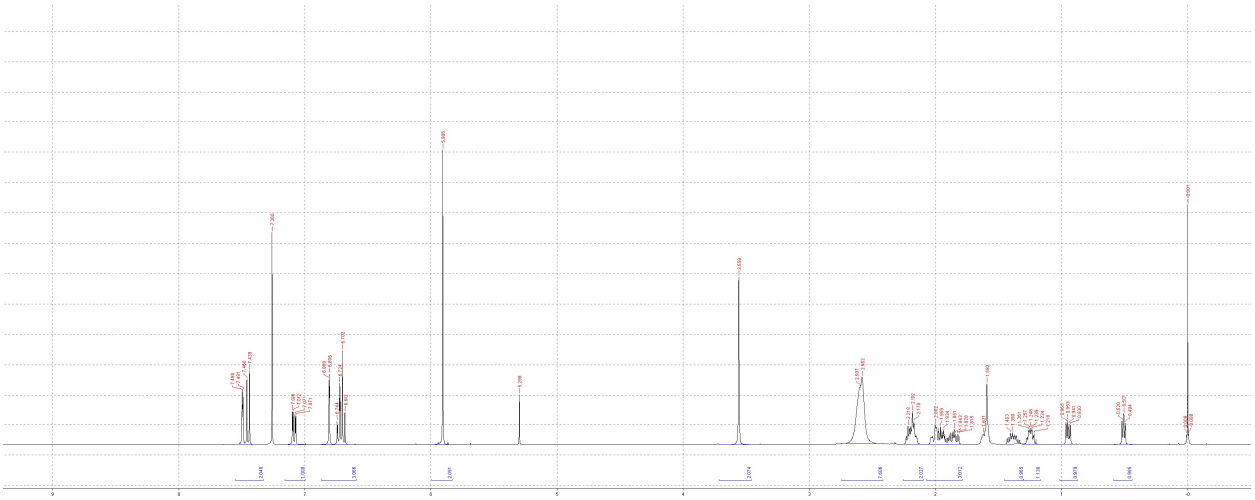

COSY NMR spectra:

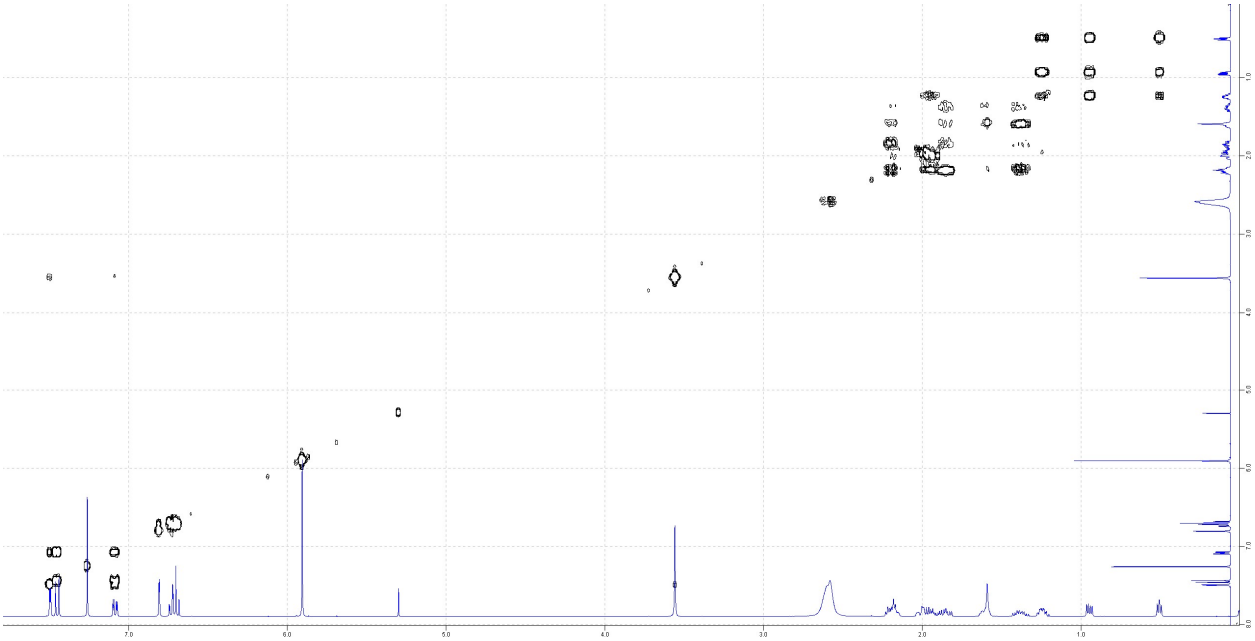

NOSY NMR spectra:

ISOMER 3

1-[6-(1,3-benzodioxol-5-yl)norcaran-3-yl]-4-[(2-bromo-5-chloro-phenyl)methyl]piperazine - Isomer 3: (0.419 g, 0.832 mmol, 100 mass%, 12.0% yield). 2D NMR analysis shows relative stereochemistry between cyclopropyl and piperidine as *syn*.

1H NMR spectra:

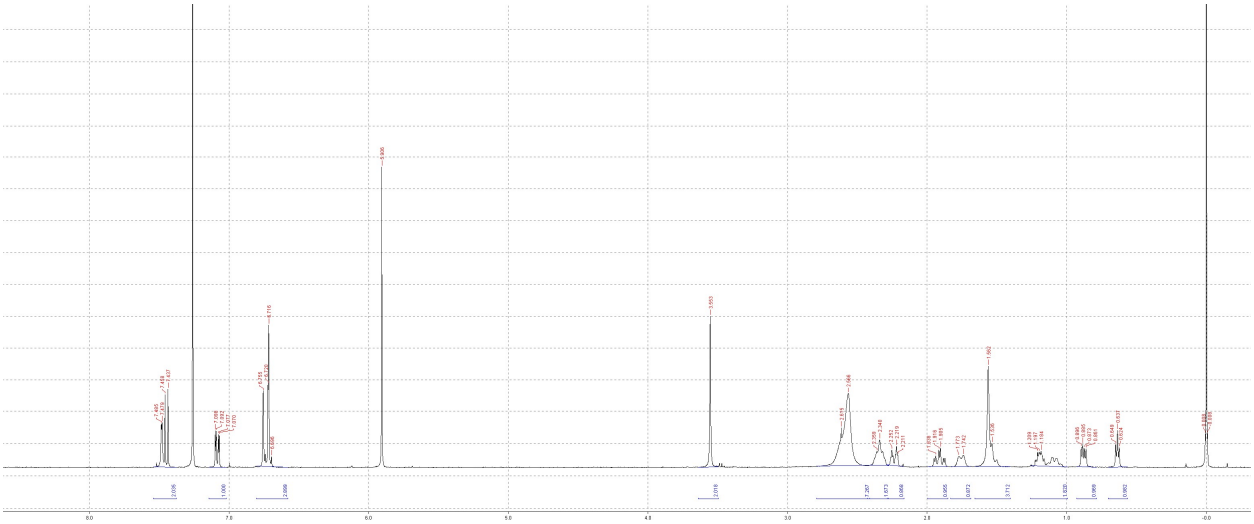

COSY NMR spectra:

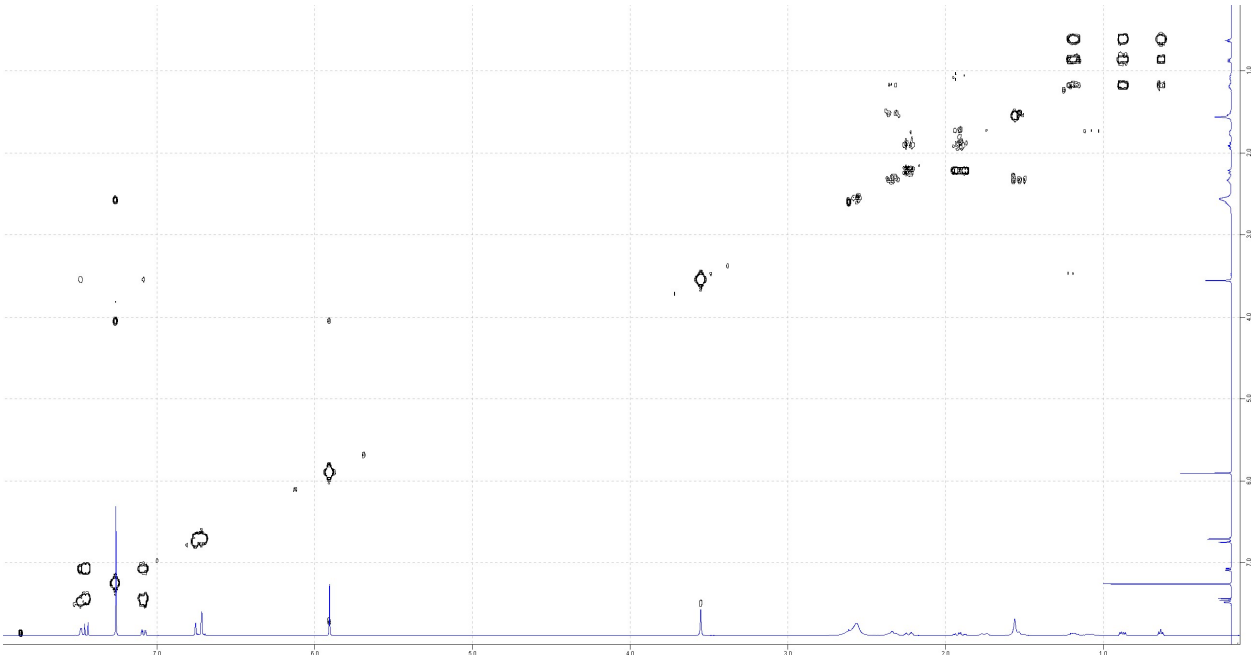

NOSY NMR spectra:

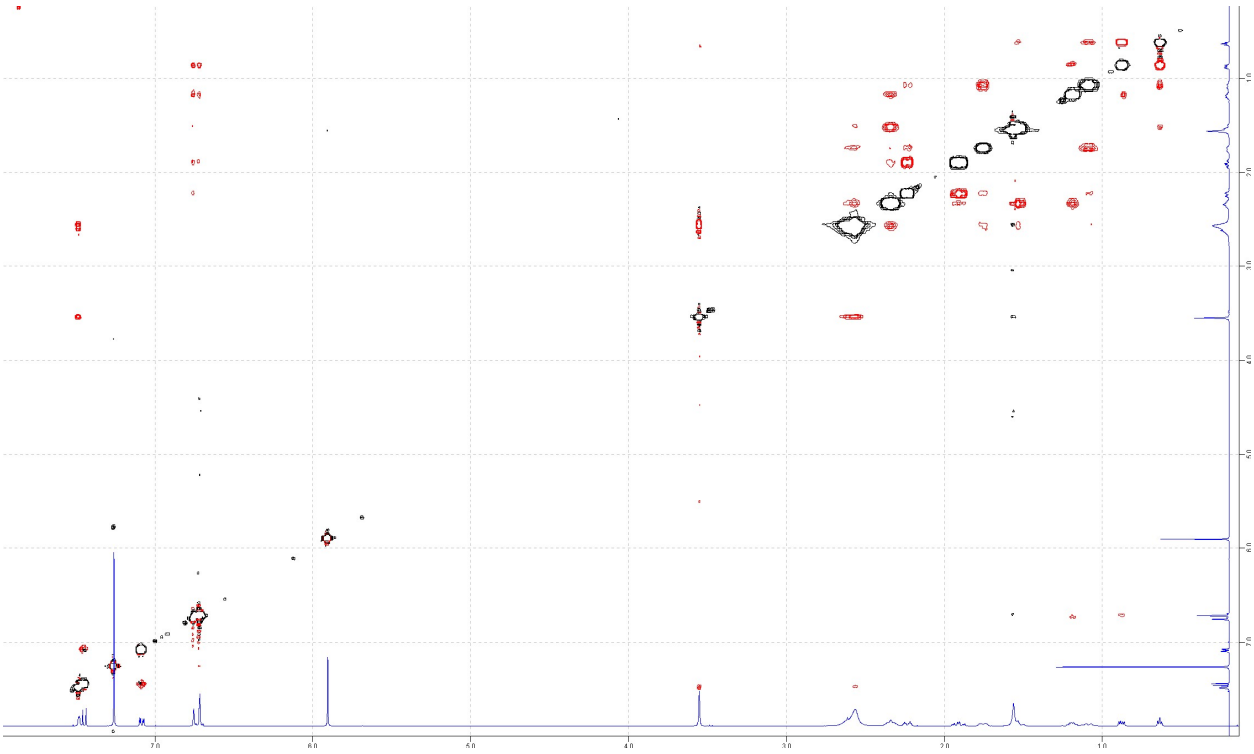

ISOMER 4

1-[6-(1,3-benzodioxol-5-yl)norcaran-3-yl]-4-[(2-bromo-5-chloro-phenyl)methyl]piperazine - Isomer 4:

(0.362 g, 0.718 mmol, 10.4% yield). 2D NMR analysis shows relative stereochemistry between cyclopropyl and piperidine as *syn*.

1H NMR spectra:

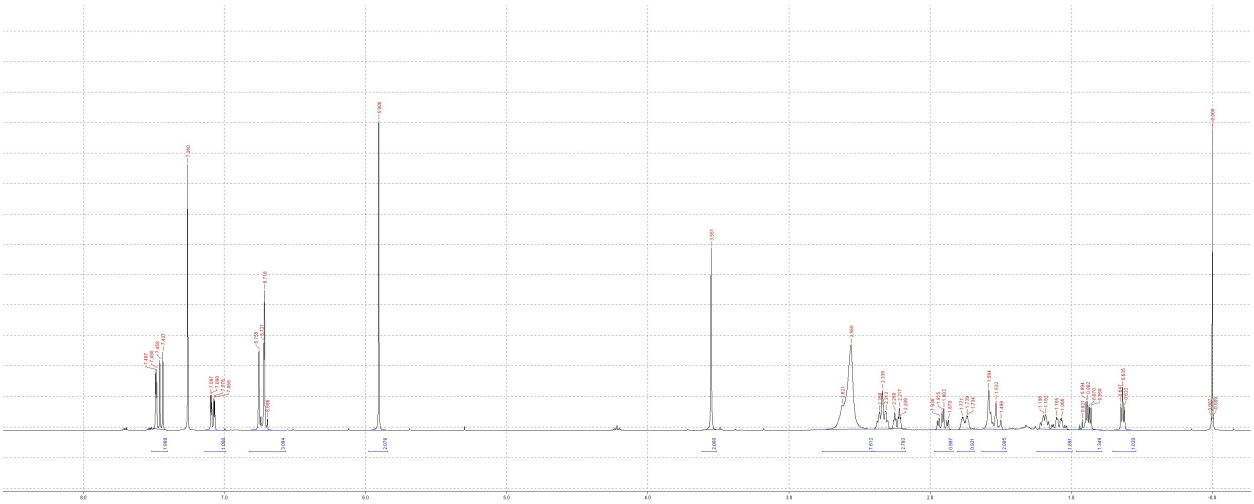

COSY NMR spectra:

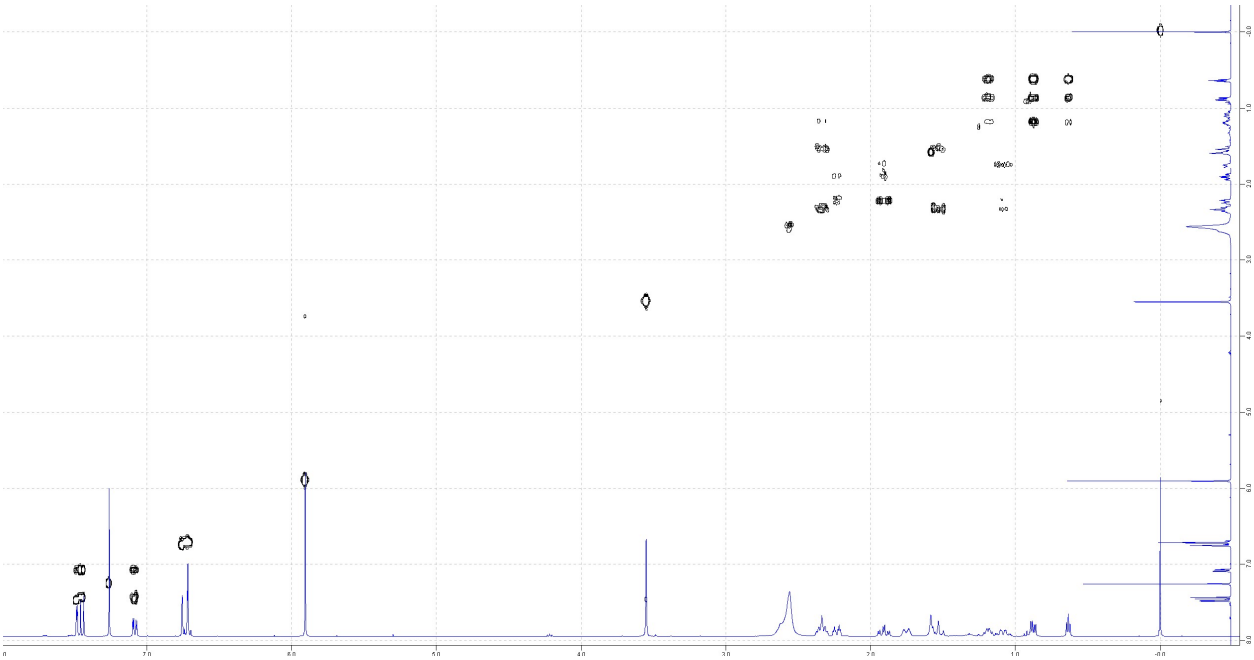

NOSY NMR spectra:

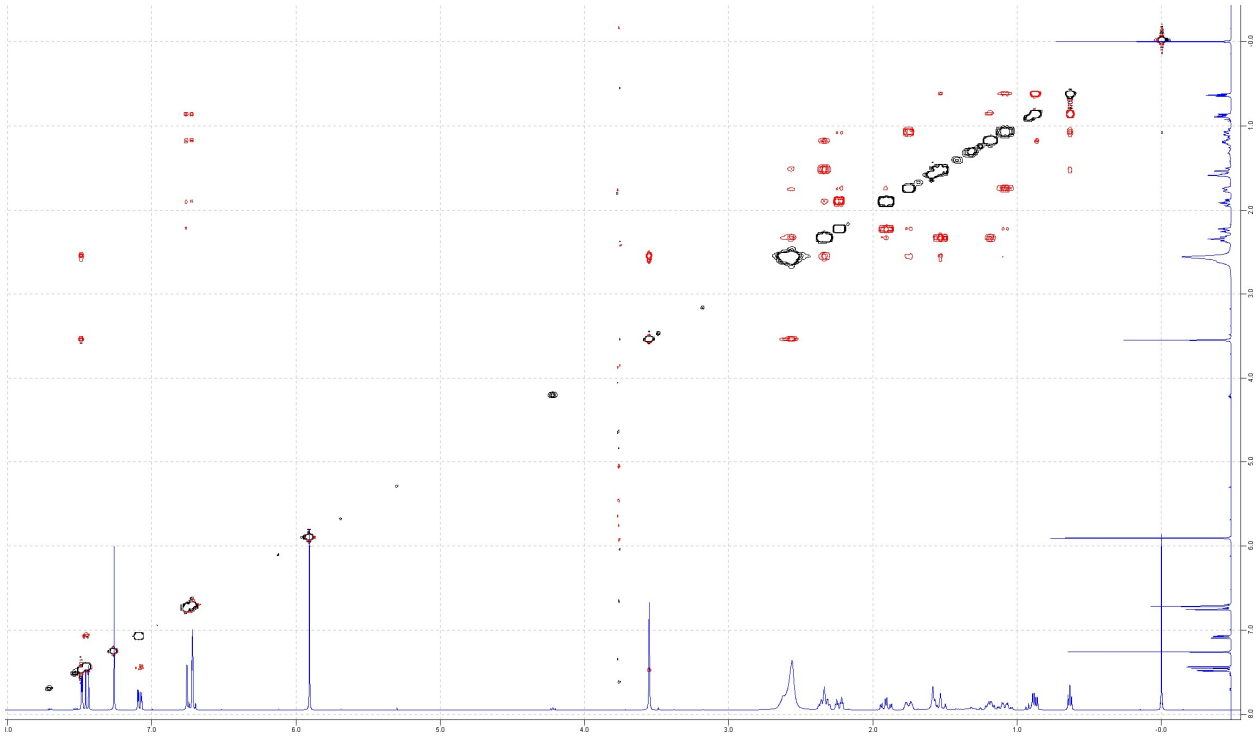

Table S1. D1 PAM activity of Compound A stereoisomers.

Cpd	hD1 PAM EC50 (nM)	Emax	n
ISOMER 1	3510 ± 356	96%	2
ISOMER 2 (BMS-A1)	1240 ± 148	96%	3
ISOMER 3	6060 ± 1480	88%	3
ISOMER 4	7310 ± 1800	98%	3

Table S2. Best-fit parameters for data in Fig. 3 (D1 PAM interactions in the absence of dopamine). Parameters for DETQ CRCs in the presence of <5 μM MLS6585 or <1.25 μM BMS-A1 had poorly defined confidence intervals and are omitted from this table.

DETQ CRC

	EC50(nM)			Hill Coefficient			Bottom (%)			Top (%)		
MLS6585 (nM)	Mean		SE	Mean		SE	Mean		SE	Mean		SE
80000	32	±	6	1.69	±	0.44	1.2	±	0.1	4.7	±	0.1
40000	36	±	6	1.46	±	0.29	0.2	±	0.2	4.9	±	0.1
20000	43	±	7	1.38	±	0.27	0.3	±	0.2	5.4	±	0.2
10000	54	±	12	1.63	±	0.53	0.3	±	0.2	3.9	±	0.2
5000	76	±	14	1.28	±	0.28	0.1	±	0.1	2.5	±	0.1

DETQ CRC

	EC50(nM)			Hill Coefficient			Bottom (%)			Top (%)		
BMS-A1 (nM)	Mean		SE	Mean		SE	Mean		SE	Mean		SE
40000	70	±	12	1.12	±	0.19	1.0	±	0.4	15.0	±	0.5
20000	37	±	8	0.89	±	0.17	0.6	±	0.6	13.6	±	0.5
10000	73	±	27	0.73	±	0.20	0.4	±	0.7	12.6	±	0.9
5000	37	±	4	0.73	±	0.20	0.6	±	0.2	10.3	±	0.2
2500	71	±	12	1.18	±	0.14	0.1	±	0.1	2.5	±	0.1
1250	225	±	115	2.10	±	0.64	0.0	±	0.1	0.7	±	0.1

BMS-A1 CRC

	EC50(nM)			Hill Coefficient			Bottom (%)			Top (%)		
MLS6585 (nM)	Mean		SE	Mean		SE	Mean		SE	Mean		SE
40000	5400	±	200	1.79	±	0.13	0.4	±	0.1	19.8	±	0.3
20000	3500	±	200	1.75	±	0.14	0.7	±	0.2	23.8	±	0.4
10000	3500	±	100	2.87	±	0.22	0.3	±	0.2	26.6	±	0.4
5000	3900	±	200	3.05	±	0.40	0.1	±	0.3	24.4	±	0.5
2500	5100	±	300	3.66	±	0.85	-0.1	±	0.2	14.9	±	0.5
1250	5200	±	400	3.58	±	1.04	-0.2	±	0.2	8.1	±	0.3
625	7200	±	900	3.45	±	1.07	-0.3	±	0.1	4.1	±	0.3
310	5700	±	500	5.79	±	3.24	-0.1	±	0.1	2.6	±	0.1
156	5600	±	800	4.41	±	2.76	-0.1	±	0.1	1.8	±	0.1
78	7600	±	1000	2.95	±	0.95	-0.1	±	0.0	1.5	±	0.1
39	8000	±	1400	2.88	±	1.22	-0.1	±	0.0	1.2	±	0.1
20	13700	±	6800	1.45	±	0.75	-0.3	±	0.0	0.9	±	0.3
9.8	7600	±	1700	2.67	±	1.33	-0.3	±	0.0	0.8	±	0.1

DETQ CRC

	EC50(nM)			Hill Coefficient			Bottom (%)			Top (%)		
	Mean		SE	Mean		SE	Mean		SE	Mean		SE
5 µM MLS6585	93	±	17	0.96	±	0.15	0.1	±	0.1	2.3	±	0.1
5 µM BMS-A1	77	±	17	0.84	±	0.15	0.1	±	0.2	6.5	±	0.4
5 µM BMS & MLS	19.6	±	1.3	1.30	±	0.10	10.4	±	0.9	63.8	±	0.8